ANALYSIS OF THE EFFECT OF DEEP EXCAVATION ON BEHAVIOUR OF AN ADJACENT PILE IN SAND USING 3D FINITE ELEMENT METHOD

SAMEH ASHOUR

T.C.
BURSA ULUDAĞ UNIVERSITY
GRADUATE SCHOOL OF NATURAL AND APPLIED SCIENCES

ANALYSIS OF THE EFFECT OF DEEP EXCAVATION ON BEHAVIOUR OF AN ADJACENT PILE IN SAND USING 3D FINITE ELEMENT METHOD

Sameh ASHOUR
0000-0003-0590-0203

Assist. Prof. Dr. Yeşim Sema ÜNSEVER
(Supervisor)

MSc THESIS
DEPARTMENT OF CIVIL ENGINEERING

BURSA – 2021

ÖZET

Yüksek Lisans Tezi

KUM ZEMİNDEKİ BİR DERİN KAZININ KOMŞU KAZIĞIN DAVRANIŞI ÜZERİNDEKİ ETKİSİNİN 3D SONLU ELEMANLAR METODU İLE ANALİZİ

Sameh ASHOUR

Bursa Uludağ Üniversitesi
Fen Bilimleri Enstitüsü
İnşaat Mühendisliği Anabilim Dalı

Danışman: Dr. Öğr. Üyesi Yeşim Sema ÜNSEVER

Bitişik kazık davranışı üzerindeki derin kazı etkisinin incelenmesi, kazığın hizmet verebilirliğini ve stabilitesini değerlendirmek için önemli bir konudur. Bu çalışmada, bitişik yüklü tekil kazık üzerindeki derin kazının etkisi doymuş kohezyonsuz zeminde 3D sonlu elemanlar yöntemi kullanılarak araştırılmıştır. Literatürde bulunan santrifüj deney sonuçları kullanılarak sonlu elemanlar modelinin doğrulanmasından sonra kazı derinliği, kazıktan kazı alanına olan mesafe ve kazık başı tipi gibi kazık davranışına en fazla etki eden faktörler üzerinde parametrik bir çalışma yapılmıştır.

Bu çalışmada, kazık uzunluğuna göre kazı derinliğinin kazık davranışı üzerinde önemli bir etkiye sahip olduğu sonucuna varılmıştır. H_e/L_p üç durumu arasında, H_e/L_p= 0.5 durumu maksimum eğilme momentine neden olurken, H_e/L_p= 1.5 durumu maksimum kazık yanal sapmasına neden olmuştur. Ayrıca kazıktan kazıya olan mesafe de kazık tepkisi üzerinde önemli bir etkiye sahiptir ve kazıkta aktive olan eğilme momenti 9 m mesafeden sonra etkisini kaybetmiştir. Ayrıca kazık başlığı tipinin de kazık davranışı üzerinde önemli bir etkisi olduğu görülmüştür. Hem kazık başına uygulanan iş yükünün arttırılması hem de kazık boyunun arttırılmasının yanal kazığın davranışı üzerinde önemli bir etkiye sahip olmadığı görülmüştür.

Anahtar Kelimeler: Tekil kazık, Derin kazı, Kumlu zemin, Sonlu elemanlar yöntemi, PLAXIS 3D

2021, x+78 sayfa.

ABSTRACT

MSc Thesis

ANALYSIS OF THE EFFECT OF DEEP EXCAVATION ON BEHAVIOUR OF AN ADJACENT PILE IN SAND USING 3D FINITE ELEMENT METHOD

Sameh ASHOUR

Bursa Uludağ University
Graduate School of Natural and Applied Sciences
Department of Civil Engineering

Supervisor: Assist. Prof. Dr. Yeşim Sema ÜNSEVER

The influation of deep excavation on adjacent pile behaviour is an important issue to ensure its serviceability and stability. In this paper, the effect of deep excavation on an adjacent loaded single pile in saturated cohesionless soil was investigated by 3D finite element method. After verification of finite element model using centrifuge test results found in literature, a parametric study was conducted by varying the most influence factors on pile behaviour such as excavation depth, distance from pile to the excavation and pile head type.

It was concluded that the excavation depth with respect to pile length has a significant effect on pile response. Among the three cases of H_e/L_p, the case of H_e/L_p= 0.5 induced the maximum bending moment while the case of H_e/L_p= 1.5 induced the maximum pile lateral deflection. Moreover, the distance from the pile to the excavation site has also a significant influence on pile response and the induced bending moment in pile is inconsiderable after 9 m distance. Also, it is observed that the pile head type has an important effect on the pile behaviour especially in case of rigid head case. Both increasing the working load applied on pile and increasing the pile length do not have a significant effect on the lateral behavior of pile.

Key words: Single pile, Deep excavation, Sandy soil, Finite element method, PLAXIS 3D

2021, x+78 pages.

ACKNOWLEGDEMENT

I would like to thank my esteemed advisor Yeşim ÜNSEVER who has never spared her knowledge and support throughout my graduate education.

To my mother's pure soul, who did not leave me during this period, who was and still is the main source of support and inspiration.

I would like to express my endless thanks to my family who have supported me in every period of my life.

Sameh ASHOUR
28/09/2021

CONTENTS

Page

SYMBOLS and ABBREVIATIONS

Symbols	Definition
A_p	Pile area
A_s	Outer pile shaft area
B_{max}	Maximum base resistance
c	Undrained cohesion of soil
D	Influence zone distance
d_p	Pile diameter
E	Young's modulus
E_{oed}	Primary oedometer stiffness
E_{50}	Triaxial compression stiffness
E_{ur}	Unloading/reloading stiffness
E_p	Elastic modulus of pile
E_i	Initial stiffness
E_pI_p	Flexure rigidity of pile
$e_{initial}$	Initial void ratio
f_s	Unit skin friction
f_i	Unit friction resistance at any depth
G	Shear modulus
H_e	Final depth of excavation
H_e/L_p	Excavation depth to pile length ratio
K	Bulk modulus
K_a	Active pressure coefficient of Rankine
k	Strut stiffness
K	Effective earth pressure coefficient
K_0	Pressure coefficient of Rankine at rest
K_0^{nc}	K_0 value for normal consolidation
L_p	Pile length
M	Tangent of the critical state line
m	Power for stress-level dependecy of stiffness
N	Friction coefficient between soil and pile
N_b	Soil stability number
N_{cb}	Critical stability number against basal heave
N_q^*	Factor of load capacity
P	Pile perimeter
p_{ref}	Reference stress for stiffness
P_h	Applied load on pile
P_a	Atmospheric pressure
Q_{ult}	The ultimate bearing capacity of a pile
Q_s	Skin friction load
Q_b	End bearing load
Q_L	Limiting value for point resistance
q	Deviatoric stress
q_p	Unit end bearing

q_a	Asympototic value of the shear strength
q_f	Ultimate deviatoric stress
q'	Effective vertical stress
R_f	Failure ratio
s_u	Undrained shear strength of soil
T_{max}	Maximum skin resistance
X	Distance from the excavation to the pile (center to center)
y_{max}	Maximum lateral soil movement
σ_a	Active earth pressure
ϕ'	Effective friction angle of
δ_v	Ground surface settlement
V_s	Volume of lateral movement of soil mass
κ	Cam-clay swelling index
δ_{vm}	Maximum ground surface settlement
σ	Stress
ε	Strain
ν	Poisson's ratio
λ	Cam-clay compression index
ψ	Dilatancy angle
$\Delta_{ph,max}$	Maximum pile head settlement at the pile ultimate capacity
γ_{sat}	Saturated unit weight of soil
γ_{dry}	Dry unit weight of soil
μ_s	Friction coefficient between soil and pile
σ'_v	Vertical effective stress

Abbreviation Definition

BM	Bending moment
BEM	Boundary element method
FOS	Factor of safety
FEM	Finite element method
GSS	Ground surface settlement
HS	Hardening soil model
LD	Lateral deflection
MCC	Modifiy Cam Clay
MC	Mohr-Coulomb model

FIGURES

Page

TABLES

Pages

1. INTRODUCTION

1.1. Problem Statement

Due to rapid urbanization and lack of lands in urban spaces, the problem of converge buildings began to emerge, so in these areas, the construction of high-rise structures with basements and construction of underground facilities (such as tunnels and metro stations) besides the pre-constructed buildings are common. High-rise buildings absolutely require deep excavation to reach to the formation level. One of the problems of deep excavation in urban spaces is the ground settlements of nearby buildings due to the lateral movement of the soil towards the excavation side and effective stress release in the lateral soil. Obviously, lateral soil movement will cause extra bending forces, lateral movement, and settlements on surrounding pile-supported buildings. The researchers have been interested in this topic because of the higher effects of deep excavation on ground movements and, as a result, on nearby existing buildings.

The underground infrastructures and excavating works for basement construction beside existing buildings absolutely will lead to lateral movements in surrounding soil due to stress relief. This situation requires to take into account the safety of these buildings as well as ensure the stability of the foundations that support them (Soomro et al. 2019, Liyanapathirana and Nishanthan 2016, Finno et al. 1991 and Goh et al. 2003).

According to field measurement data, the braced deep excavation has a significant effect on adjacent piled foundation buildings, and the pile responses to soil movements should be taken into account during designing (Zhang et al. 2018).

In this study, three-dimensional numerical analyses will be carried out to obtain new insights into pile response to adjacent deep excavation in sand by using 3D PLAXIS finite element program.

1.2. Research Objectives

The goal of this study is evaluating the behavior of a loaded single pile owing to a propped deep excavation in sandy soil by PLAXIS 3D finite element (FE) program. The pile response will include the bending moment, lateral deflection and settlement of the pile.

For this purpose, 3D finite element model will be developed, which takes account of small-strain stiffness by using PLAXIS 3D program. The validated model will be utilized to study the most influencing factors on the pile behavior (i.e., excavation depth, distance from the pile to excavation, pile head type, pile length and working load applied on pile).

The principle objectives of this study are:

1. Validation of the finite element model that will be used in analysis using the centrifuge test results taken from literature.
2. Establishing of the pile response due to changing
   -the depth of excavation.
   -the distance from the pile to the excavation face.
   -the pile length.
   -the working load (*P*) applied on the head of pile.
   -the pile head type.

1.3. Research Methodology

The following methodology is followed in this study to achieve the research objectives:

a) Summarizing the available literature related to the modelling of the pile response due to adjacent deep excavation to understand the used constitutive soil models and material models.

b) Development of (FE) model using PLAXIS 3D: Non-linear three dimensional finite element model will be created to simulate the pile response due to adjacent deep excavation using the commercial finite element modeling software (PLAXIS 3D) as follows:

I. Identifying the single pile properties.
II. Modeling of single loaded pile with specific structural properties in the sand to identify its ultimate bearing capacity by establishing load-settlement curve.
III. Developing the finite element model by modeling the soil, pile, diaphragm wall and struts. Also, determine the boundary conditions of model, wall-soil and pile-soil interaction.
IV. The developed model will be verified by using the centrifuge test results taken from literature.
V. Carrying out the nonlinear analysis.
VI. Getting the analysis results.

2. THEORETICAL BASICS and LITERATURE REVIEW

2.1. Pile Foundations

Piles can be defined as a structural elements made from steel, timber , or concrete to transmit the loads to a deep level of soil (Bowles 1996). These structural members are used to transmit the loads that applied on a structure to the more stiffer and compact soil layers and rocks (Tomlinson and Woodward 2008). This type of foundations began to appear as a simple wood pile in old civilizations to overcome the problems of founding in soft soils; such as those near lakes and rivers, and in very highly compressible clay deposits (Tomlinson and Woodward 2008, Zeevaert 1957).

2.1.1. General uses of piles

The piles are used in the following commonly cases (Das 2011):

1. If there is one or more weak soil layers of high compressibility, the piles here used to transfer the loads to a nearest strongest layer of rock layers (Figure 2.1.a, b).
2. When the structure subjected to horizontal forces as shown in Figure 2.1.c.
3. When an expansive soil is exposed to swelling and shrinking exists in the soil layers (Figure 2.1.d).
4. When uplift-prone foundations, such as transmission towers, basement mats, and offshore platforms, are used below the water table (Figure 2.1.e) .
5. When the abutments and piers of the bridge are built to avoid the loss of bearing capacity (Figure 2.1.f).

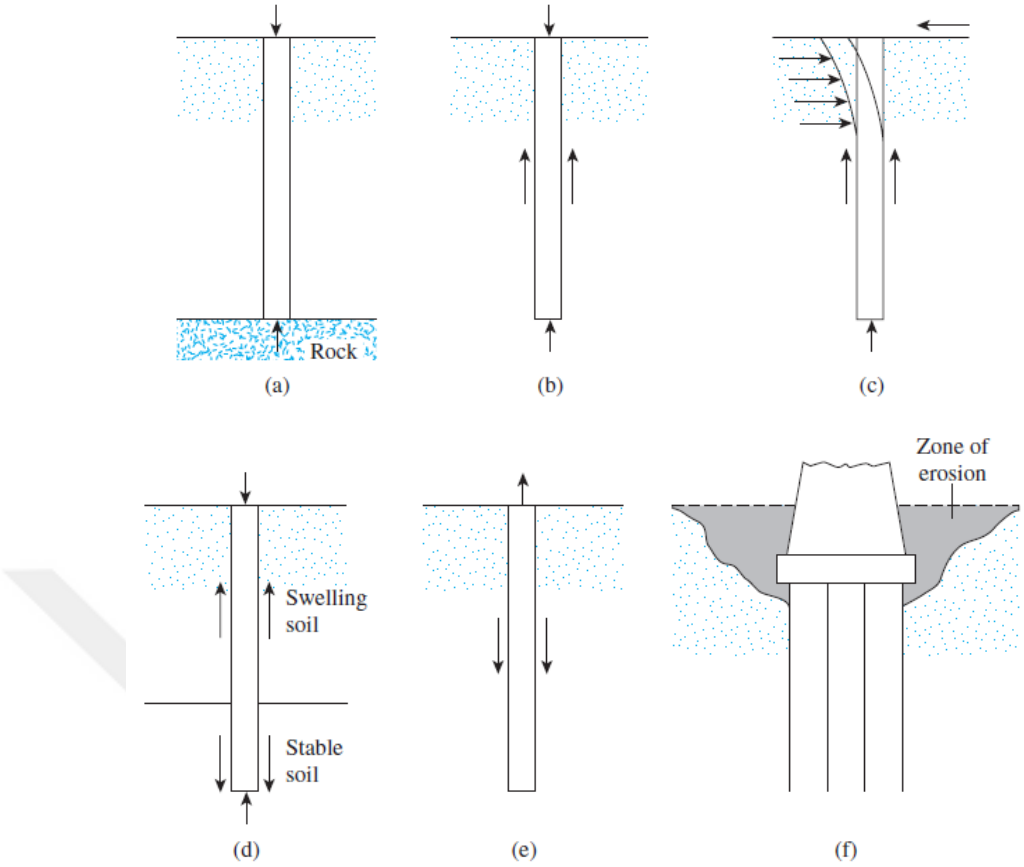

Figure 2.1. Conditions necessitating the use of piles as a foundation (Das 2011).

2.1.2. Types of piles

The primary function of piles is safely transfer load applied to the superstructure to the stronger ground layers. Pile bearing capacity is divided into two parts: skin friction and end bearing capacity. (Poulos and Davis 1980). The contribution of tip resistance and friction resistance of the pile bearing capacity varies based on the subsoil condition and the pile type. Venkatramaiah (2006) and Das (2011) mentioned that piles are classified based on different ways, such as the function, used material, method of installation and others.

The types of piles according to function can be divided into the following:

a) If the soil bearing capacity that will support the structure is too low and has high compressibility, the pile is extended to the deeper strong layer with a high bearing capacity and the loads from the superstructure are carried with the pile end resistance. This type of piles are called **end piles** (Figure 2.2.a).

b) If the soil layer with a high bearing capacity is very deep, the superstructure loads are carried along the pile length by the side friction forces that will occur in the soft and loose soil layers. This type of pile is called **friction pile**. The friction piles are extended by the length until sufficient friction force is obtained (Figure 2.2.b).

c) If the soil has a swelling-shrinking structure or the structure will be subjected to high overturning moment, the stability of the structure is increased by using tensile piles in the foundations against the hydrostatic pressure or torque of the structure. These piles driven into the ground are called **pull piles** (Figure 2.2.c).

d) If the ground is loose and split grain, tightening is done by driving piles in order to provide the density that can carry the loads from the superstructure. **Compaction piles** are the piles that are used for this purpose. (Figure 2.2.d).

e) Piles used in coastal structures and shoring systems carry horizontal loads such as lateral soil loads, wave load and impacts by the ships. For this purpose, **horizontally loaded piles**. (Figure 2.2.e).

f) In the foundations of structures that undergo excessive horizontal loads such as offshore platforms, **inclined piles** that carry loads both horizontally and vertically are used (Figure 2.2.f).

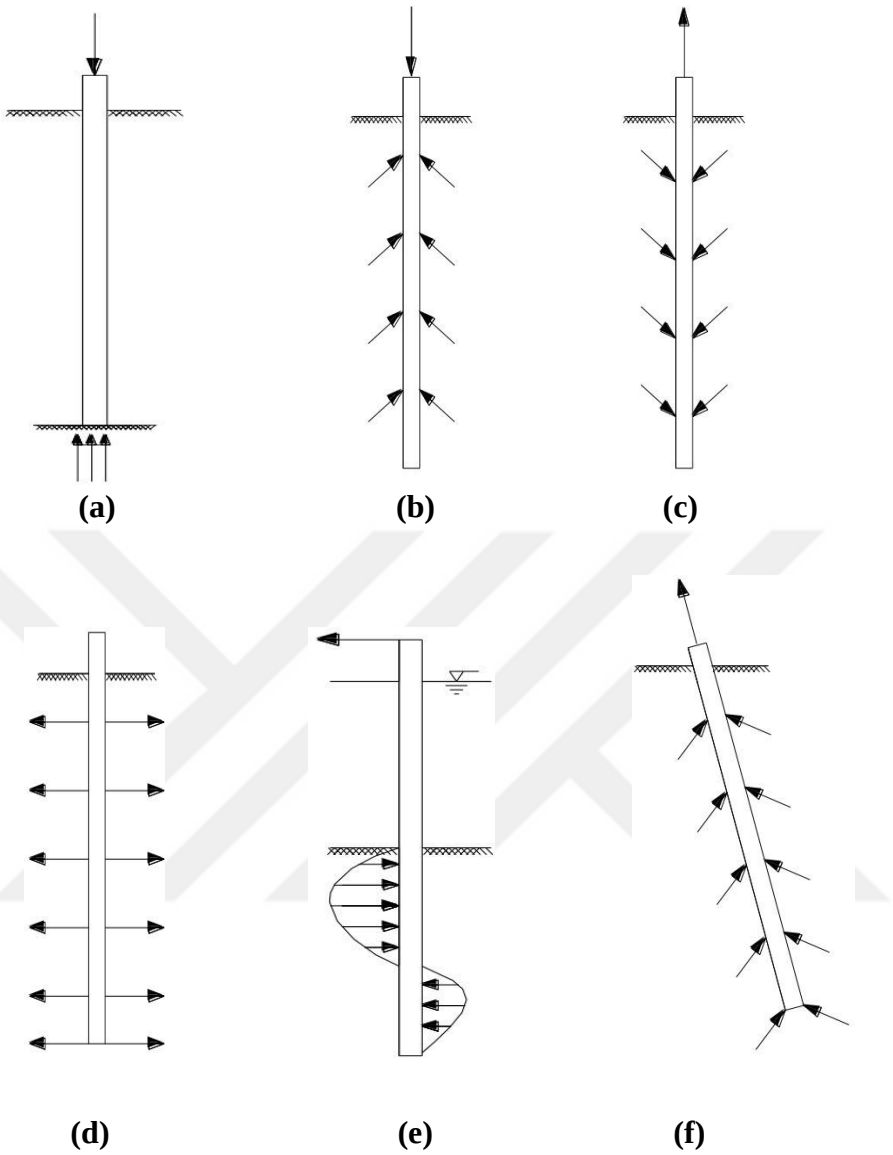

Figure 2.2. The types of piles according to function (Akbay 2009).

2.1.3. The ultimate bearing capacity of pile

The ultimate bearing capacity of a pile is known as the maximum load that the pile can carry without failure or excessive ground settlement. The allowable load is multiplied by a relevant safety factor. The bearing capacity of a pile is primarily established by the

type of soil it passes through and/or rests on, the technique of installation, and the pile dimensions (Venkatramaiah 2006).

The ultimate bearing capacity of a pile is computed by using the below equation:

$$Q_{ult} = Q_s + Q_b \tag{2.1}$$

Where; Q_s is skin friction load and Q_b is end bearing load (or point resistance). In sand, the end bearing, Q_b tends to predominate, whereas in soft clay, the skin friction, Q_s is usually dominant. Skin friction capacity can be calculate as follow:

$$Q_s = f_s . A_s \tag{2.2}$$

where; A_s is the outer pile shaft area (m^2) and f_s is the unit skin friction (kN/ m^2).

End bearing load can be calculate as follow:

$$Q_b = q_p . A_p \tag{2.3}$$

where; q_p is the unit end bearing (kN/ m^2) and A_p is the pile end area (m^2).

The final equation of ultimate bearing capacity of pile is:

$$Q_{ult} = (f_s . A_s) + (q_p . A_p) \tag{2.4}$$

It can be obtained on the allowable capacity by dividing the ultimate capacity to the factor of safety (FS).

2.2. Analysis of Laterally Loaded Piles

Beside supporting vertical loads, the piles also support lateral loads which produce shears and moments. Wide loads, earth pressures on retaining walls, and seismic loads

are all examples of lateral load sources (Coduto 2001). Axial loads cause settlements that are parallel to the pile axis, whereas lateral loads can generate displacement in any direction. The axial loads are transferred through side friction and toe resistance, as shown in Figure 2.3, but the lateral loads are transferred through soil lateral bearing.

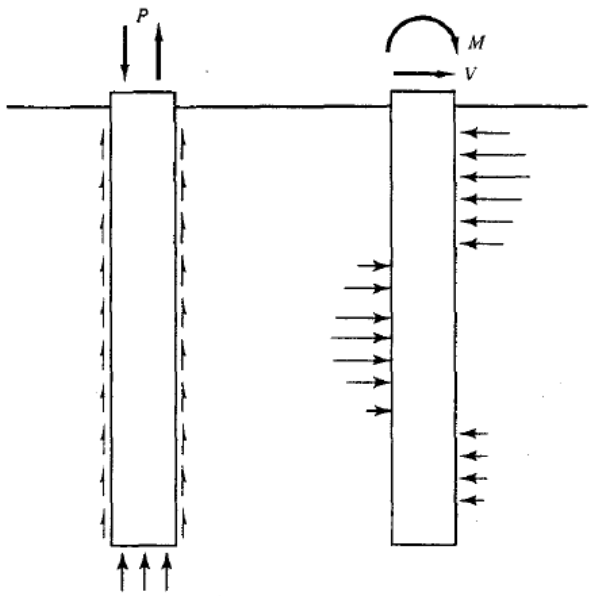

Figure 2.3. Mechanism of transfer of lateral and axial loads from the deep foundation to the ground (Coduto 2001).

2.2.1. Rigid analysis method

The first analysis method used to solve lateral load problems in piles foundations is the rigid analysis method, that accepts the pile as completely rigid. This method use static equations to determine the distribution of soil ultimate resistance, which brings the pile to a state of equilibrium. However, in this analysis method the rotation of the piles is neglected, and simple definitions were used for soil resistance. This analysis method was used by Broms (1964a, 1964b, 1965) to derive equations for estimating the loading that develops the ultimate bending moment.

2.2.2. Depth of fixity analysis method

During the 1960s and 1970s, the depth of fixity analysis method was applied. This method predicts that the pile bends due to horizontal load. Furthermore, it is assumed that the pile is fixed at a depth of (L_f) below the ground surface. This allows to deal with the real pile as a cantilever with total length equal to summation of (L_u) and (L_f), as shown in Figure 2.4. The solution satisfies that the deflection and rotation at the top of equivalent pile as well as the buckling load are the same for the real pile, and these can be determined from the basic principles of static equations (Davisson 1970).

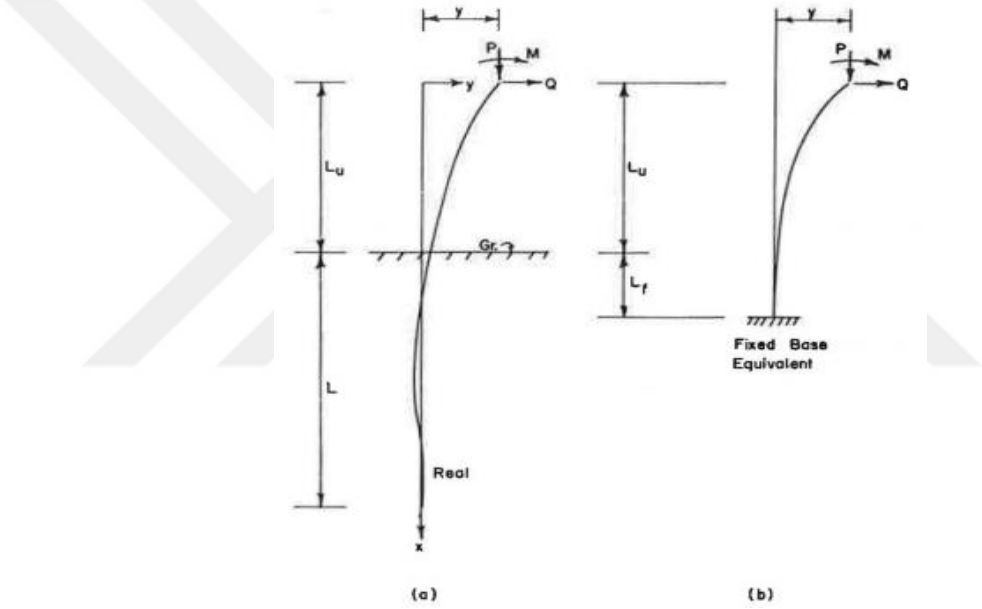

Figure 2.4. Partially embedded pile (Davisson 1970).

2.2.3. Norigid soil-structure interaction analysis method

This method is designed to take into account the foundation's flexural rigidity, soil reaction to lateral stresses, and soil-structure interaction. This method depends on the finite element method (FEM) and the p-y method.

The (FEM) works by decomposing the pile and soil into individual elements and determining stress-strain parameters to each one. The response of these elements to imposed loads is then taken into account. Because the soil is more complicated and the stress-strain relationship is nonlinear, the efficiency of this method is dependent on accurate assigning of the element properties (Coduto 2001).

P-y method employs a sequence of nonlinear "springs", in order to describe the soil-structure interaction. It's relatively easy to use than the finite element method (FEM), but it's not as accurate. As a result, load test results with full scale are utilized to calibrate it.

2.3. Excavation Methods and Lateral Supporting Systems

There are different excavation methods used in the construction site. The most appropriate approach is determined by a number of considerations, including the construction budget, availability of construction equipment, the permissible work period, adjacent excavations, construction site area, adjacent building conditions, and foundation types of these buildings. Among these methods, the most commonly utilized method is the braced excavation method.

2.3.1. Braced excavation method

To resist the earth pressure applied to the retaining wall, horizontal struts are constructed in front of the wall in this approach. Wales are also used to transfer pressure to the struts; end braces are used to shorten the span of wales without increasing the number of struts; corner braces are used to reduce the distance between struts; and center posts are used to support the struts, as shown in Figure 2.5. Although struts and center posts may obstruct the excavation process, the braced approach is the most generally utilized method and may be applied to any depth or width of excavation.

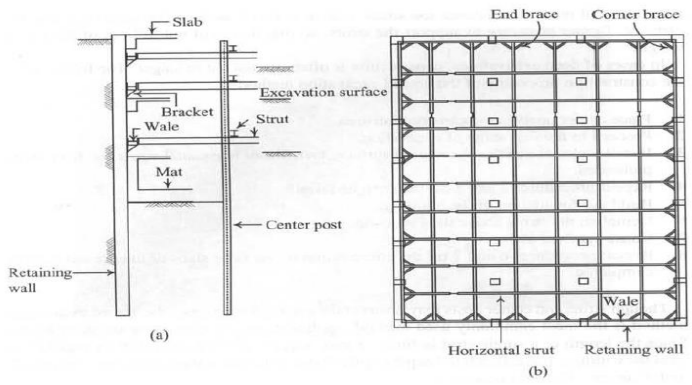

Figure 2.5. Braced excavation method: (a) profile (b) plan (Ou, 2006).

2.3.2. Diaphragm walls

Diaphragm wall is a type of retaining wall used to support the lateral soil due to excavation. It was adopted first in Italy in the 1950s, then has been widely used around the world. Although this method is very expensive and requires advanced construction equipments, it is considered one of the most used methods as a retaining wall owing to the its several advantages. Table 2.1. shows the advantages and shortcomings of diaphragm wall.

Table 2.1. Advantages and shortcomings of diaphragm walls (Ou, 2006)

Advantages	shortcomings
Low vibration and noise, high rigidity and relatively small wall deflection	Advance equipments are needed, long period of construction and high cost
Adjustable thickness and wall depth	The huge equipment occupies large area
Good sealing capability	Not used in gravelly grounds
Can be used as a permanent structure	When dealing with quick sand, it is hard to construct.

2.4. Braced Excavations Subjected to Earth Pressures

Rankine and Coulomb theories use the general wedge theory to determine earth pressure. However, because the analysis does not provide a relationship to estimate the change of lateral earth pressure with depth, the distribution of soil pressure technique differs from the conventional Rankine and Coulomb earth pressure theories in the shoring systems that support the excavation. Figure 2.6.a illustrates the envelope of apparent lateral pressure diagrams for cutting sands developed by Peck (1969), and the active earth pressure for sand is determined by equation 2.5:

$$\sigma_a = 0.65\ \gamma H\ K_a \tag{2.5}$$

where:

γ : unit weight of sand

H : height of the cut

K_a: the active pressure coefficient of Rankine = $tan^2(45- \frac{\phi'}{2})$

ϕ': effective friction angle of sand

Figure 2.15.b illustrates the pressure graphs for cuts in soft to medium clays and stiff clays, as indicated by Peck (1969). The following condition apply to the soft to medium clay pressure envelope:

$$\frac{\gamma H}{c} > 4 \tag{2.6}$$

where, c = undrained cohesion ($\phi = 0$).

The pressure, σ_a, is the larger of following two equation:

$$\sigma_a = \gamma H\ [(1- \frac{4c}{\gamma H})] \tag{2.7}$$

$$\sigma_a = 0.3\ \gamma H \tag{2.8}$$

The pressure envelops for cuts in stiff clay is shown in Figure 2.6.c and is given by the following equation:

$$\sigma_a = 0.2\ \gamma H \text{ to } 0.4\ \gamma H \quad \text{(with an averge of } 0.3\ \gamma H) \tag{2.9}$$

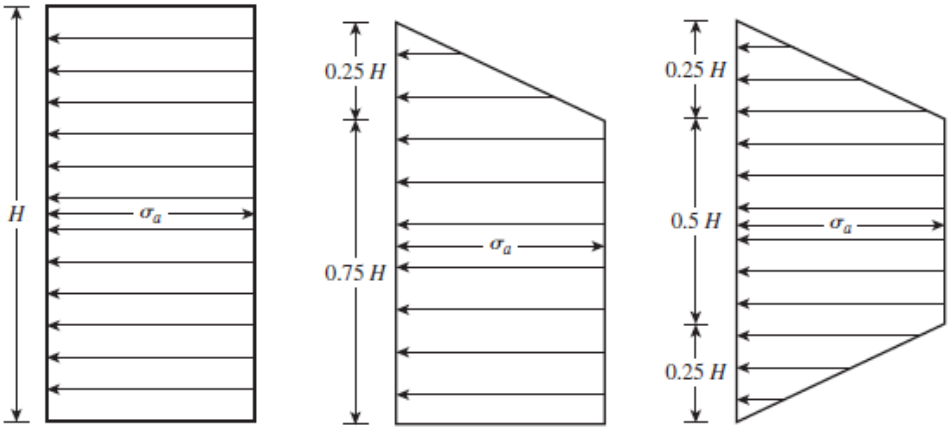

Figure 2.6. Peck's apparent pressure envelope for (a) sand cuts, (b) soft to medium clay cuts, and (c) stiff clay cuts (Peck 1969).

It is important to remember the following when using the pressure envelops in Figure 2.6:

- They can be used in excavations that are deeper than 6 meters.
- They're based on the idea that the water table is below the cut bottom.
- The pore water pressure in sand is assumed to be zero.
- Pore water pressure doed not considered since clay is assumed to be undrained.

2.5. Estimation of Excavation-Generated Ground Surface Settlements

Unbalanced pressures and earth removal inside the excavation site causes ground movements behind the retaining wall. Many factors, including excavation depth, excavation geometry, quality of construction, ground condition, groundwater level, excavation process, support system and the settlement magnitude and distribution can effect the movement. Because it is difficult to produce an accurate method derived only from theoretical approaches, the majority of ground settlement prediction systems rely on field measurements (Hsieh and Ou 2000) .

2.5.1. Peck's (1969) method

Peck (1969) proposed a method based on field observations to estimate the ground surface settlement owing to excavation. He used the monitoring results from case studies in Chicage and Oslo to create a curve for settlement of ground surface (δ_v) and distance from the wall (d) for various soil types, as illustrated in Figure 2.7. According to the approach, there are three types of soil.

Zone I: Sand and soft to stiff clay, with average workmanship

Zone II: Very soft to soft clay

1. Clay depth below the excavation's bottom is limited.
2. There is a significant amount of clay below the excavation's bottom.

Zone III: Very soft to soft clay to a significant depth below the excavation bottom and with $N_b > N_{cb}$

where:

N_b: the soil stability number

$$N_b = \frac{\gamma H}{s_u} \tag{2.10}$$

N_{cb}: the critical stability number against basal heave

γ: soil unit weight

H: depth of excavation

s_u : undrained shear strength of soil

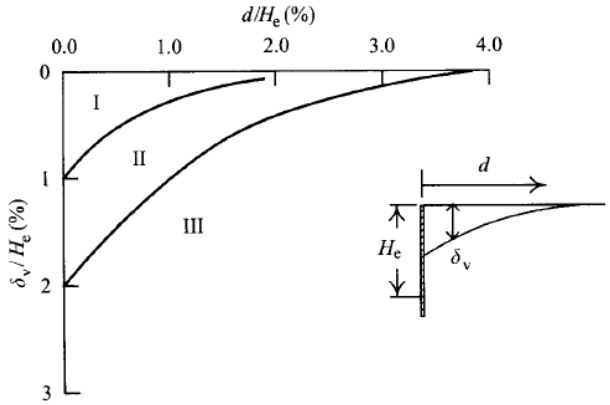

Figure 2.7. Estimating ground surface settlement using Peck's approach (1969).

2.5.2. Bowles's (1988) method

As illustrated in Figure 2.20, Bowles (1988) provided a procedure for calculating the spandrel-type settlements profile owing to excavation. The following are the steps:

- Using a beam elastic foundation method or a FEM, calculate the lateral deflection of the wall.
- Calculate the lateral movement volume of soil mass (V_s).
- Determine the influence zone (D) using the following approach proposed by Caspe (1966):

$$D = (H_e + H_d) \tan(45 - \frac{\phi}{2}) \quad (2.11)$$

where:

H_e: final excavation depth

H_d : equals to excavation width (*B)* for cohesive soil, for cohesionless soil

$$H_d = 0.5Btan(45 + \frac{\phi}{2}) \quad (2.12)$$

ϕ: internal friction angle of the soil

- Assume that the maximum ground surface settlement (δ_{vm}) occurs at the wall:

$$\delta_{vm} = 4\ V_s/D \tag{2.13}$$

- It is assumed that the settlement curve is parabolic. The settlement (δ_v) at the distance (l_x) can be described as in the equation 2.14:

$$\delta_v = \delta_{vm}\ (\frac{l_x}{D})^2 \tag{2.14}$$

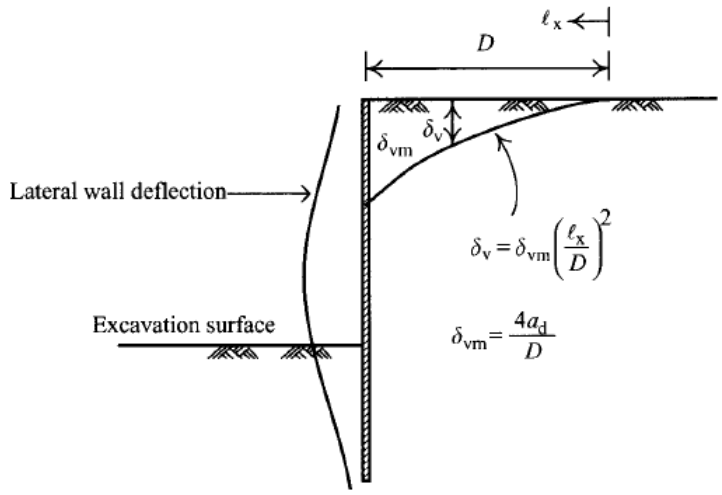

Figure 2.8. Bowles's method (1988) for estimating ground surface settlement.

2.5.3. Clough and O'Rourke's (1990) method

Clough and O'Rourke (1990) developed different curves to calculate ground settlements due to excavation for different soils based on many case studies. Figures 2.9.a,b illustrate the ground settlement profiles for sand and stiff to very stiff clay, respectively. The ground surface settlement pattern is a triangle in both cases, with influence ranges of ($2H_e$) and ($3H_e$) for sand and stiff clay, respectively, where (H_e) is the final depth of excavation and maximum settlement occurs at the retaining wall (i.e., spandrel surface profile). The ground surface settlement pattern for an excavation in soft to medium clay is trapezoidal, with the maximum settlement occurring in the range of $0 \leq d/H_e \leq 0.75$, then decreasing to zero in the range of $0.75 \leq d/H_e \leq 2.0$.

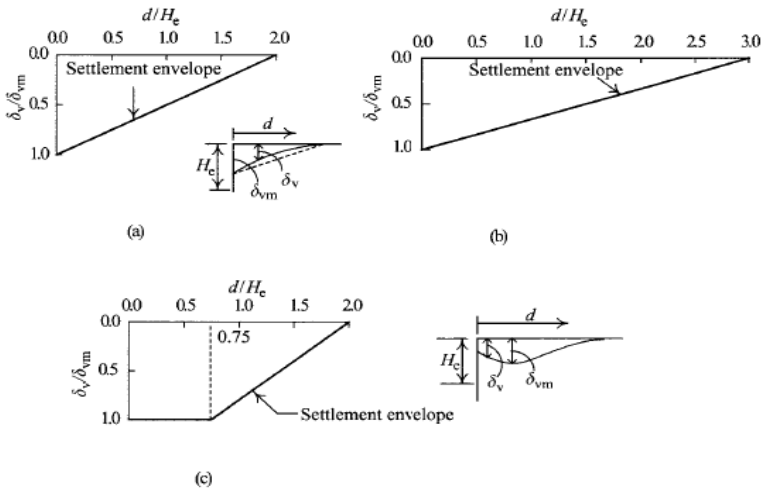

Figure 2.9. Ground surface settlement for (a) sand, (b) stiff to very stiff clay, and (c) soft to medium soft clay, as suggested by Clough and O'Rourke (1990).

2.6. Overview on PLAXIS 3D Finite Element Program

2.6.1 Finite element method

FEM is a numerical methodology for solving difficult engineering challenges and applications with a high level of precision. After the expansion of computer numerical analysis, FEM method became widely employed around the world, and it is now applied in all engineering branches. It is based on the geometry of a problem with specific boundary conditions. Defined geometry is divided into a number of sub-components known as "finite elements," which are joined together by nodes. Each node has a number of freedom degrees, which corresponds to the problem unknowns. FEM is widely used in geotechnical engineering to build and analyze geotechnical structures in a safe and cost-effective approach, as well as to evaluate the behavior of these structures in the face of potential risks.

2.6.2. PLAXIS 3D program

PLAXIS 3D is a three dimensional finite element program which employed for geotechnical analysis and design. Users can easily create a geometry model using the program's flexible graphical interfaces. Two subprograms (Input and Output program) make up the user interface (PLAXIS 3D Reference Manual 2020).

The input program is a pre-processor for defining the problem's geometry, creating the finite element mesh, and defining calculation phases. The geometry modes and calculation modes are the two different groups of modes. The following geometry modes are available:

Soil mode: The definition of soil properties into the program is considered as the most necessary step, because of an incorrect description of soil layer parameters surely will lead to incorrect analysis results. It is common to perform some in-situ and lab experiments on soils in order to establish their parameters and properties, which will then be entered into the program, resulting in more accurate modeling results. This mode defines the soil stratigraphy, soil material properties, general levels of ground water, and the initial conditions of the soil layers.

There is simple soil models available in PLAXIS, such as linear elastic and Mohr-Coulomb model are completely plastic models. While the advanced material models, are recommended for simulating actual soil behavior (PLAXIS Material Models Connect Edition V20).

- Linear elastic model: Hooke's law of isotropic linear elasticity is employed in this model. It is insufficient for simulating the soil behavior. It is mostly employed to simulate the rigid structures. Hook's law describes the linear relationship between the stress (σ) and strain (ε), as shown in the equation below:

$$\dot{\sigma'} = M\,\dot{\varepsilon} \tag{2.15}$$

Where (M) is a material stiffness matrix. Hook’s law also can be given by the equation:

$$\begin{bmatrix} \dot{\sigma}'_{xx} \\ \dot{\sigma}'_{yy} \\ \dot{\sigma}'_{zz} \\ \dot{\sigma}'_{xy} \\ \dot{\sigma}'_{yz} \\ \dot{\sigma}'_{zx} \end{bmatrix} = \frac{E'}{(1-2\nu')(1+\nu')} \begin{bmatrix} 1-\nu' & \nu' & \nu' & 0 & 0 & 0 \\ \nu' & 1-\nu' & \nu' & 0 & 0 & 0 \\ \nu' & \nu' & 1-\nu' & 0 & 0 & 0 \\ 0 & 0 & 0 & \frac{1}{2}-\nu' & 0 & 0 \\ 0 & 0 & 0 & 0 & \frac{1}{2}-\nu' & 0 \\ 0 & 0 & 0 & 0 & 0 & \frac{1}{2}-\nu' \end{bmatrix} \begin{bmatrix} \dot{\varepsilon}_{xx} \\ \dot{\varepsilon}_{yy} \\ \dot{\varepsilon}_{zz} \\ \dot{\gamma}_{xy} \\ \dot{\gamma}_{yz} \\ \dot{\gamma}_{zx} \end{bmatrix} \quad (2.16)$$

The effective Young's modulus is (E'), and the effective Poisson's ratio is (ν').

The relationship between Young's modulus (E) and various stiffness moduli, such as shear modulus (G), bulk modulus (K), and oedometer modulus (E_{oed}), according to Hook's law, is as follows:

$$G = \frac{E}{2(1+\nu)} \quad (2.17)$$

$$K = \frac{E}{3(1-2\nu)} \quad (2.18)$$

$$E_{oed} = \frac{(1-\nu)E}{(1-2\nu)(1+\nu)} \quad (2.19)$$

- Hardening Soil Model (HS): The (HS) model is a complex model that models the soil behavior using the Mohr-Coulomb failure criterion. This model is based on the hyperbolic model of soil stress-strain curves derived from triaxial test results. In the hyperbolic model, the elastoplastic stress-strain behavior of soil is described by different modulus of elasticity values for loading and unloading conditions. With its approximation of stiffness, this model differs from the MC model. This model may be used to simulate the behavior of a variety of soils, including sands, gravels, clays, and silts.

The following parameters used to describe the soil in this model:

- ϕ : effective angle of internal friction

- c_{ref} : reference cohesion
- E_{50} : Secant stiffness at a stress level of 50% in a standard drained triaxial test
- E_{oed} : primary oedometer loading tangent stiffness (default $E_{oed} \approx E_{50}$)
- E_{ur} : unloading/reloading stiffness (default $E_{ur} \approx 3E_{50}$)
- ν_{ur} : Unloading-reloading Poisson's ratio (default ν_{ur} = 0.2)
- p_{ref} : refence stress for stiffness (default p_{ref} = 100 stress units)
- K_{oNC} : K_o value for normal consolidation (default K_{oNC} = 1-sinϕ)
- R_f : failure ratio q_f/q_a (default R_f = 0.9)
- m : power for stress-level dependecy of stiffness

In primary loading for a conventional drained triaxial test, Figure 2.10 illustrates the hyperbolic relationship between the vertical strain (ε_1) and the deviatoric stress (q). This figure is described by Equation (2.20):

$$-\varepsilon_1 = \frac{1}{E_i} \frac{q}{1-q/q_a} \qquad \text{for: } q < q_f \tag{2.20}$$

Where (q_a) is the asympototic value of the shear strength given by Equation (2.23), and (E_i) the inital stiffness. (E_i) is related to (E_{50}) and given by the following equation:

$$E_i = \frac{2E_{50}}{2- R_f} \tag{2.21}$$

The confining stress dependent stiffness modulus for primary loading is (E_{50}), which is provided by the equation below.

$$E_{50} = E_{50}^{ref} \left(\frac{c \cos\phi - \sigma_3' \sin\phi}{c \cos\phi + p^{ref} \sin\phi}\right)^{\mathrm{m}} \tag{2.22}$$

The reference stiffness modulus (E_{50}^{ref}) corresponds to the reference stress (p^{ref}). The default setting in PLAXIS is (p^{ref} = 100 kN/m2). The minor principal stress, (σ_3'), which is the confining pressure in a triaxial test, determines the actual stiffness.

The ultimate deviatoric stress, (q_f) is defined by the following equation :

$$q_f = (c \cot \phi - \sigma_3') \frac{2 \sin \phi}{1 - \sin \phi} \tag{2.23}$$

and $$q_a = \frac{q_f}{R_f} \tag{2.24}$$

Another stress-dependent stiffness modulus is employed for the unloading and reloading stress path:

$$E_{ur} = E_{ur}^{ref} \left(\frac{c \cos \phi - \sigma_3' \sin \phi}{c \cos \phi + p^{ref} \sin \phi} \right)^{m} \tag{2.25}$$

where:

E_{ur}^{ref} : the reference Young's modulus for unloading and reloading, corresponding to the reference pressure (p^{ref}). In many practical issues it is common to use (E_{ur}^{ref}) equal to $(3E_{50}^{ref})$.

In PLAXIS, the value of m can be taken equal to 1.0 for soft soils and for other soils varies between 0.5~1.0.

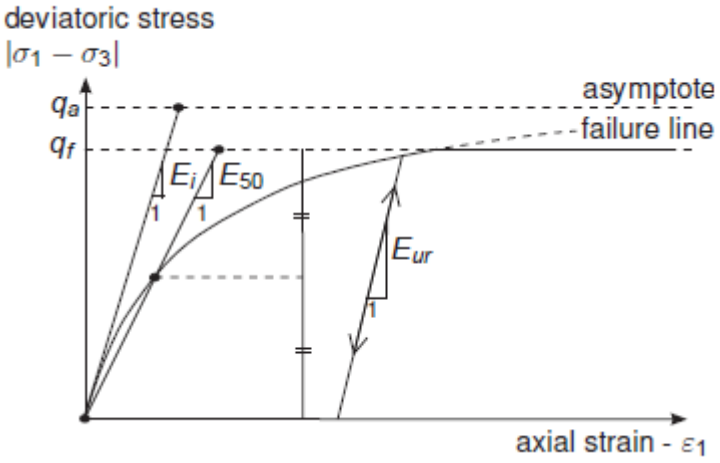

Figure 2.10. A strandrad drained triaxial test with a hyperbolic stress-strain relationship in primary loading (PLAXIS Material Manual 2020).

Structures mode: In this mode the user defines the geometric entities, the structural elements and forces. Some of structural elements are as follows:

- Fixed-end anchors: It's a point element that's fixed on one side and attached to a structure on the other. It is defined by the normal stiffness and the analogous length which is the distance in the longitudinal direction between the anchor connection point and the fictitious point. It can be used to support retaining walls by simulating anchors or props.

- Plates: The plates are actually shell elements, which are structural elements used to describe thin two dimensional ground structures with high bending stiffness (flexural rigidity).

- Embedded beam: The embedded beam is a structural object composed of beam elements with special interface elements that allow the beam to interact with the earth around it. It can be used to simulate pile, rock bolt or grout body.

- Interfaces: Interfaces are joint elements that are used to model the interaction between soil and structure. They can also be generated next to plate or geogrid elements, or between two soil volumes, to simulate the connection area between a plate and the surrounding soil.

Mesh mode: In this mode, the geometry model is discretized and a FE mesh is created.

Flow conditions mode: In this mode, defined water levels can be provided and adjusted in addition to water levels obtained by the water condition defined in the soil mode.

Staged construction mode: The geometry model properties can be changed and parts of it can be activated or deleted. In this mode, the project is calculated.

The output software is a post-processor that plots the curves of output values at the desired mesh points or at the selected elements. This program provides to user a possibility of showing a cross section in any element and understand the genetrated stresses, displacements and forces in these elements.

2.7. Summarizing of Literature Reviews

Soomro et al. (2019) studied the single pile responses owing to adjacent excavation in saturated soft clay. 3D numerical studies by using software ABAQUS are employed in the analyses. To model the excavation above, next to, and below the pile toe, three cases of excavation depth (H_e) relative to pile length (L_p) (i.e., H_e/L_p= 0.67, 1 and 1.33) are utilized. Figure 2.11 displays the case of H_e/L_p= 1. The pile behavior was found to be strongly dependant on the final of H_e and wall embedded depth. The pile head settlement (i.e., 7.6% of the pile diameter (d_p)) was the highest in the case of H_e/L_p= 1.33, but the largest deflection at the pile toe was in the case of H_e/L_p= 0.67. (i.e., 5.0% of d_p). Furthermore, when the excavation completed, no considerable changes in the distribution axial load were observed in either case. In addition, the pile head type has a major effect on the produced bending moment, but only a slight impact on settlement. The free head caused the most pile deflection in the upper portaion in the three pile head cases. In the case of fixed head, a large bending moment (about 60% of the pile B.M. capacity of 800 kN.m) was produced. The impact of different working loads (FS = 3.0 and 1.5) on settlement of pile was significant, although the impact on bending moment was minor.

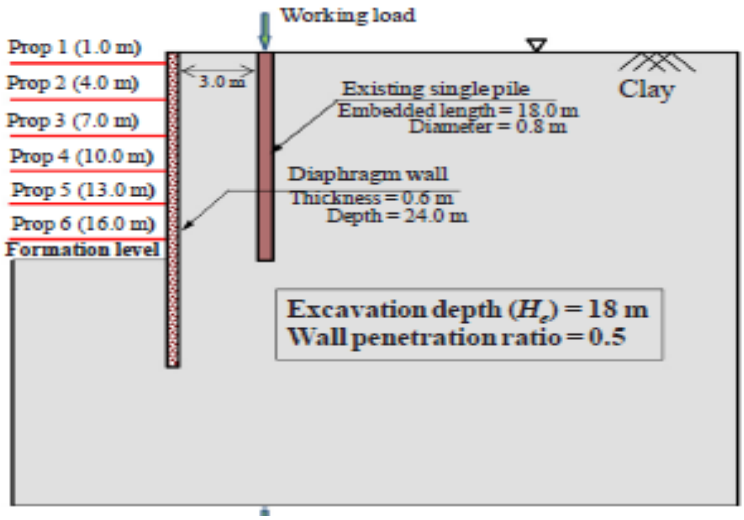

Figure 2.11. Definition of (H_e/L_p = 1) case analyzed by (Soomro et al. 2019).

Zhang et al. (2018) investigated the pile behavior during nearby excavation by varying different impact factors shown in Figure 2.12 by using the hardening small strain constitutive (HSS) model in software PLAXIS. It was found that the maximum produced LD and BM increase approximately linearly with the increasing of H_e. In addition, pile length has a significant impact on the pile behavior. Furthermore, as the distance from the excavation increases, the maximum value of LD and BM of pile decreases considerably. And it was found that the maximum LD decreases linearly with increasing of pile diameter (d_p), but the LD of pile head increases with increasing of d_p. In contrast, the pile BM's showed a significant increase with the increasing of d_p. On the other hand, the BM on the pile base are dependent on the pile head type. The pile behavior is unaffected by the axial load.

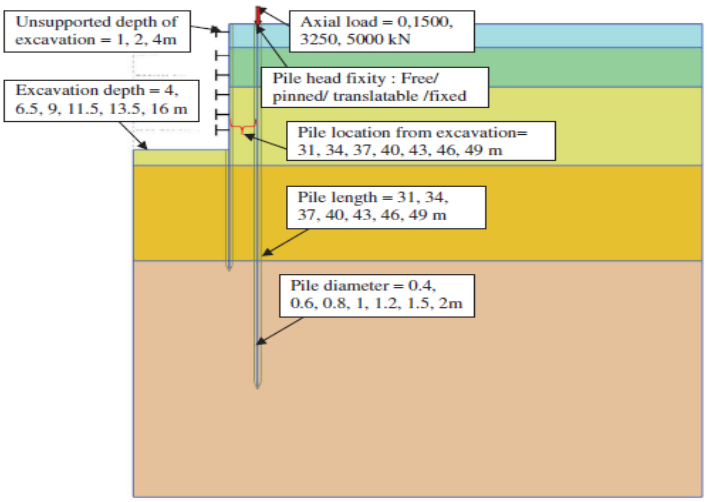

Figure 2.12. Definition of the problem analyzed by (Zhang et al. 2018).

The influence of the excavation on settlement and load transfer mechanism of 2*2 adjacent group pile in soft clay was investigated using HSS constitutive model in software PLAXIS 3D, as shown in Figure 2.13 (Shakeel and Ng 2017). The pile group settlement was found to be related to the excavation depth. The maximum settlement of pile group occurs at a distance of 0.75 times of H_e. The effect of increasing the stiffness of the supporting system on settlement is more visible in a flexiable wall than in a stiffer wall. The pile shaft resistance is mostly determined by the pile toe position in relation to the excavation level. Excessive negative pore water pressures are created in the soil as a result of excavation, and the dissipation of these pressures causes pile group long-term settlement.

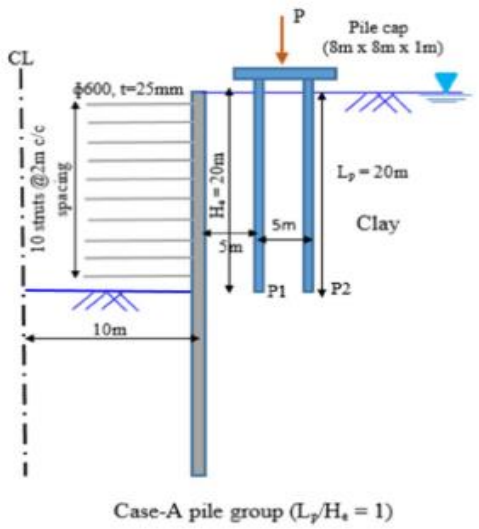

Figure 2.13. Analyzed problem (Case-A) (Shakeel and Ng 2017).

Ng. et al. (2017) utilized three centrifuge model experiments (free, pinned, and fixed-head pile) to estimate the impact of a multi-propped deep excavation in-flight on a nearby pile in dry Toyoura sand. In addition, 3D numerical analysis was used to confirm the results of the centrifuge tests. The results revealed that restricting the pile head causes a large bending moment, which may exceed the pile bending capacity. The resistance of the pile shaft decreases in the upper portion of the pile during excavation, but increases in the lower portion of the pile side to side pile toe resistance when the pile settles to achieve balance.

Liyanapathirana and Nishanthan (2016) was conducted a parametric study to determine the pile responses owing to deep excavation in clayey soil by using the software ABAQUS. Figure 2.14 shows the analyzed model, they studied the effect of excavation depth (H_e), properties of soil, support system stiffness, pile head type, and distance from pile to excavation (X) during these analyses. The results revealed that the increasing in the lateral deformation and bending moment related with the increasing of H_e. The maximum lateral deformation (LD) and bending moment (BM) are reduced exponentially when the distance X is increased. There is no significant effect on the pile behavior while the strut stiffness is larger than 10 MN/m/m, but when it declines below 10 MN/m/m, the maximum BM and LD increase. Furthermore, it was observed that pile

head fixity and strut spacing have considerable impact on pile behavior, but increasing the axial load has no major affect on the pile. Finally, by employing the study results, design charts are studied to estimate the maximum LD and BM in the pile during an adjacent excavation, however they are only valid for the analyzed problem.

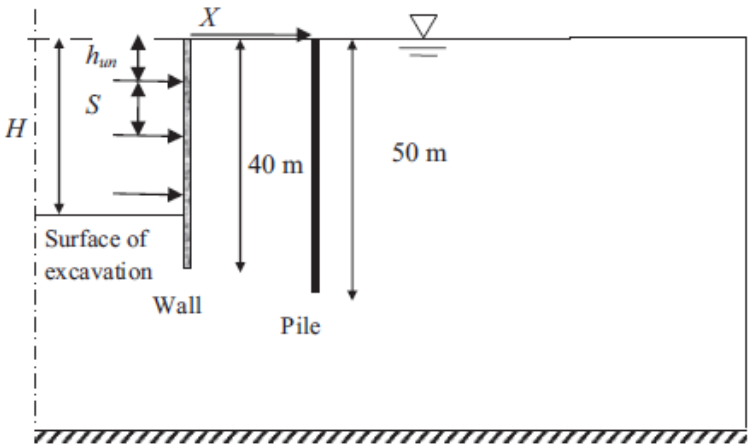

Figure 2.14. Definition of the problem analyzed by (Liyanapathirana and Nishanthan 2016).

Nishanthan et al. (2016) was used ABAQUS software to established the effect of shielding in pile groups close to unbraced and braced excavations utilizing different pile group designs and two head conditions (free and capped). The results showed that in unbraced excavation the deleterious impacts on the rear piles can be decreased by the existence of front piles. Furthermore, in unbraced excavation the deflection of pile group can reduce highly. In contrast, in braced excavation these factors have a less significant impact on pile group response.

Li et al. (2014) used MCC constitutive model in FLAC3D program to assign the influence of deep excavation near to a pile. The findings revealed that an increase in pile response corresponded to an increase in H_e. Additionally, a considerable positive BM developed at the pile head for fixed head piles, and the lateral soil pressure was the highest of the three pile head cases. The decrease in wall stiffness, on the other hand, causes a massive increase in bending moment and lateral pressure on the pile. The

maximum LD, BM, and lateral pressure all decrease as the distance between the pile and the excavation increases. Furthermore, it was observed that increasing pile stiffness minimizes pile deflection while increases moment and lateral pressure dramatically. Finally, increasing the axial pressure on a pile has only a minor impact on pile response.

Ding and Qiao (2014) conducted 2D numerical studies on pile behavior caused by deep excavation in clayey soil overlaying rock by using the software PLAXIS (Figure 2.15). A number of influence factors were investigated. The maximum LD and BM of pile were observed to increase as H_e was increased. As the entire pile was located in clayey soil, the largest deflection was observed at the pile toe, and when the pile went into rock soil layer, the maximum deflection was found at the pile head. Moreover, once the pile length reaches 12 m, increasing the length has little effect on the LD of the pile. When the pile length was increased, a significant difference in the moment profile was observed. In addition, increasing the distance from the wall (X) reduces the LD and BM of pile. Furthermore, at small pile stiffness (i.e., $0.01EI_p$ and $0.1EI_p$, where EI_p is the standard pile stiffness), the pile appeared flexible in deformation (C mode), and as stiffness increased, the pile became rigid (S mode), with no influence on deformation or moment after reaching EI_p. When the wall stiffness is increased from $0.01EI_w$ to $10EI_w$, both the lateral deformation and the moment decrease rapidly, while they change slightly when the wall stiffness is more than 10 EI_w. Finally, it was found that the thickness of the clay layer has a significant impact on the behavior of the piles as a result of excavation.

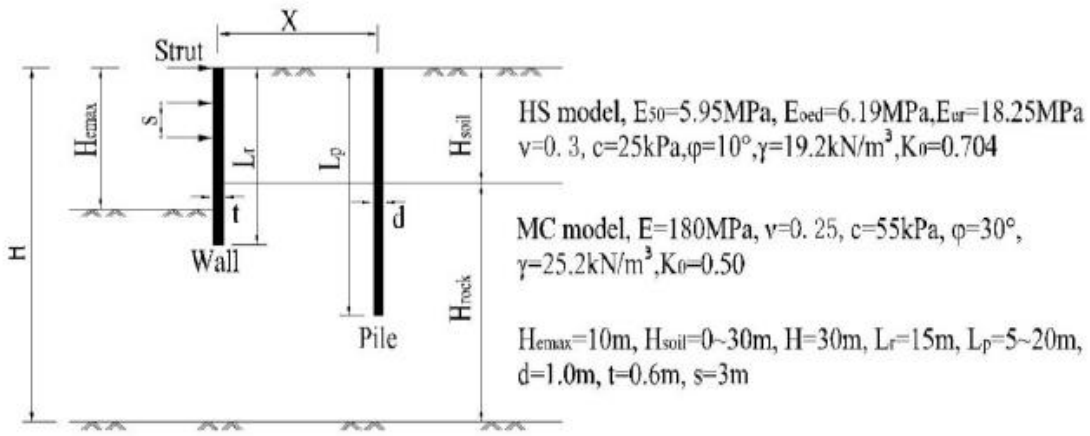

Figure 2.15. The problem analyzed (Ding and Qiao 2014).

Ong et al. (2006) was used centrifuge model tests as well as the modelling to evaluate the behavior of a single pile in clay due to unbraced excavation behind a stable wall. The excavation significantly reduced the undrained shear strength within the considerable soil deformation zone behind the wall, according to the results. Furthermore, increasing the distance from pile to excavation induced a significant decrease in pile response. The wall and soil continue to move over time owing to the dissipation of excess pore pressure after excavation is completed.

Choudhury et al. (2006) used centrifuge model tests to examine pile responses owing to sand excavation when different relative densities were considered. According to the test results, the largest bending moments are found near the pile's center and increase significantly as the pile's distance from the excavation reduces. Both magnitude of bending moments and pile deflection increase as excavation depth increases. The changing of relative density of sand from 80% to 90% at different excavation depths has an insignificant imapct on induced maximum moments in the pile.

Leung et al. (2003) conducted centrifuge model tests on pile groups with free and cap heads to specify the influence of unpropped excavation on pile group behavior in sand. It was found that the existence of front piles lead to decrease the generated effects in rear piles significantly. As well as, the existence of cap lead to reduce pile group

response. Moreover, the interior piles in four and six pile group expose to less moment, and the generated moment decreases with the increasing the number of piles.

Leung et al. (2000) used two centrifuge model tests to assign a single pile response caused by unpropped deep excavation in dense sand. The first experiment studied a stable wall. It was found that increasing the distance between the pile and the wall (X) lead to decrease the maximum LD and BM of pile exponentially. Furthermore, the type of pile head has a significant impact on pile response. The second test examined at a collapsing wall, and the results showed that the failure line of soil behind the wall extended around 3 meters from the wall to the ground surface. On piles in the failure zone, a considerable BM and head deflections were observed.

Poulos et al. (1997) expanded on previous work in the field of supported excavation (Figure 2.16). It was found that increasing the stability number led to an increase in wall and soil movements in the free-field case without a pile. In addition, as the distance from pile to excavation (X) increased, the maximum lateral soil movement (y_{max}) decreased. The profile of the BM of pile was doubly curved, with maximum values increasing as the stability number increased. In addition, the effect of major pile parameters such as undrained shear strength (c_u), stiffness of wall (EI_w), strut stiffness (k), strut spacing (s), and pile diameter (d) on pile response was examined. The pile response (LD and BM) was found to increase with (c_u), increase with stability number, increase with pile diameter, and decrease with stiffer support system.

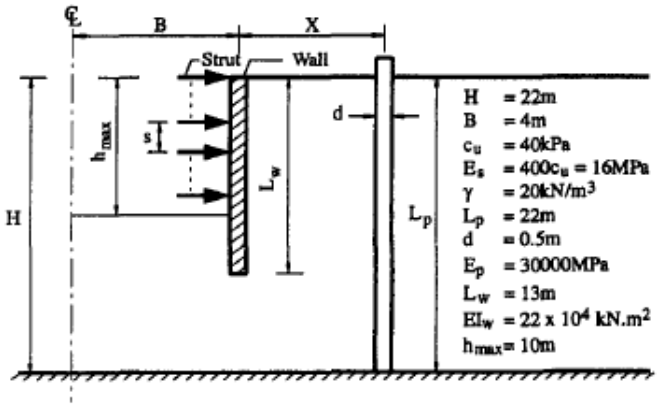

Figure 2.16. Basic problem analyzed (Poulos et al. 1997).

Poulos and Chen (1996) used a two-stage analysis which depends on utilizing FEM and BEM to assign the pile reaction owing to unsupported excavation in clay (Figure 2.17). The results revealed that as the stability number N_c (which is a function of excavation depth) increases, the maximum lateral soil movement y_{max} increases, and as the distance from the excavation edge "X" increases, y_{max} decreases, especially for the greater stability number. In the case of free field soil, it was found that the soil movement is very close to the pile deflection. The BM profile was a double curve with the maximum value increasing as the stability number increased. The design charts of maximum LD and BM of pile were then extracted based on parametric studies done on the influencing parameters (such as soil stiffness, stability number, and pile diameter). Other factors to consider are the soil tension capacity and pile head condition, both of which have a significant impact on pile response, especially pile bending moments.

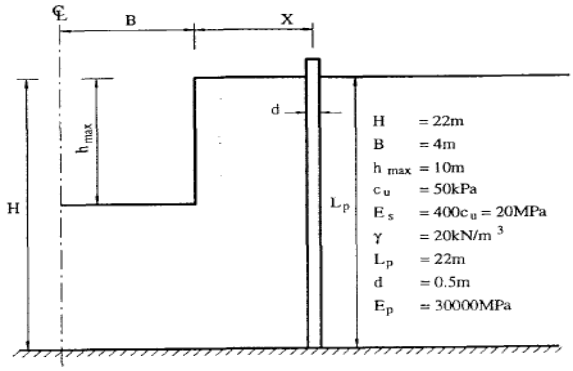

Figure 2.17. Basic problem analyzed (Poulos and Chen 1996).

3. MATERIALS and METHODS

3.1. Introduction

This thesis aims to evaluate a loaded single pile behavior due to supported deep excavation in sandy soil using PLAXIS 3D program. The parametric studies will be performed after the pile response due to nearby excavation has been validated. Various factors will be investigated such as depth of excavation, distance from the pile to excavation, pile length, vertical applied load on pile, and pile head fixity.

3.2. Validation of numerical finite element model using centrifuge test results

3.2.1. Description of the centrifuge test

The 3D finite element model that will be used in this parametric study has been validated using the centrifuge test conducted by Ong et al. (2006). The centrifuge test was carried out at a centrifuge acceleration of 50g to investigate the pile behavior owing to adjacent excavation in soft clay in case of stable retaining wall. The model container made from stainless steel with internal dimensions 540 mm long, 200 mm wide and 470 mm high. Toyoura sand was first used to fill the container to a depth of 120 mm (6 m in prototype scale), then Malaysian kaolin clay was used to fill the container to a depth of 130 mm (6.5 m in prototype scale) above the sand layer. The pile model used in the centrifuge test was from a hollow square aluminum tube and the wall model was a 3 mm-thick alumium plate. The clay layer in the excavation zone was carefully removed and replaced with a latex bag containing $ZnCl_2$ solution, which has the same density as the removed clay, after the model pile and wall were installed. During the test the excavation was carried out by draining the $ZnCl_2$ solution at 50g in six stages over two days. Ong et al. (2006) provide more details concerning the centrifuge test. Figure 3.1 and Figure 3.2 shows the cross section and plane view of the centrifuge model conducted by Ong et al. (2006) in prototype scale, respectively. Figure 3.3 shows centrifuge model setup conducted by Ong et al. (2006).

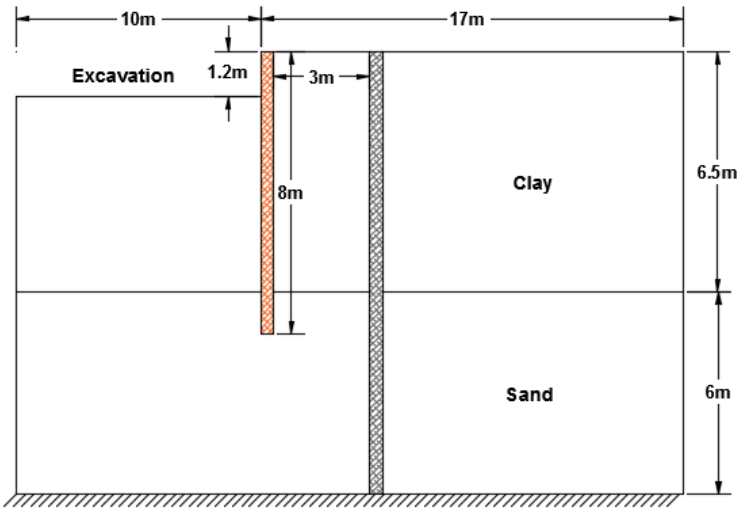

Figure 3.1. Cross section of the centrifuge model conducted by Ong et al. (2006) in prototype scale.

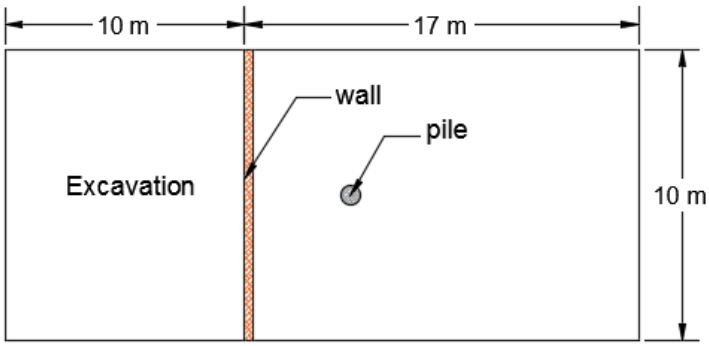

Figure3.2. Plane view of the centrifuge model conducted by Ong et al. (2006) in prototype scale.

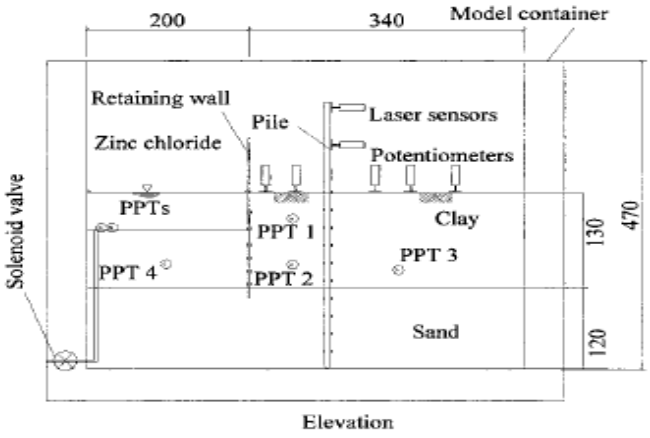

Figure 3.3. Centrifuge model setup (all dimensions in mm).

3.2.2. Materials properties used in centrifuge test

The centrifuge test was simulated with the help of the PLAXIS 3D program. The kaolin clay utilized in the centrifuge test was modeled using MCC model, which is suitable to model the normally consolidated soft soils behavior. (PLAXIS 3D Material Models V20). Table 3.1 summarized the kaolin clay properties used in the FE analysis (Ong et al., 2006, Teh et al., 2005). The Toyoura sand utilized in the centrifuge test was simulated using HS model, which is sutiable to model sandy soil behavior (PLAXIS 3D Material Models V20). Table 3.2 summarized the Toyoura sand properties used in the analyses (Leung et al., 2000).

The pile model used in the centrifuge test was from a hollow square aluminum tube which has a prototype bending rigidity, EI of 2.2×10^5 kN.m^2 this value corresponds to a 600 mm diameter cast in situ Grade 35 concrete bored pile with length of 12.5 m in protoype scale. Table 3.3 summarized the pile properties used in the analyses. The retaining wall model was a 3 mm-thick alumium plate with a prototype bending moment of 24×10^3 kN.m^2/m, this value corresponds to a FSP-IIA sheet pile with total depth of 8 m in prototype scale. The elasticity modulus of steel is 210 Mpa.

Table 3.1. MCC soil parameters for kaolin clay

Parameter	Value	Reference
Unit weight, γ (kN/m^3)	15.21	Ong et al. 2006
Cam-clay compression index (λ)	0.244	Deduced from compression and
Cam-clay swelling index (κ)	0.053	swelling index
Tangent of the critical state line (M)	0.9	Teh et al. 2005
Coefficient of permeability (m/s)	1.36×10^{-8}	Ong et al. 2006
Effective friction angle, $\phi'(°)$	23	Ong et al. 2006
K_0 value for normal consolidation, K_0^{nc}	0.6	Ong et al. 2006
Poisson's ratio, (ν)	0.3	

Table 3.2. HS soil parameters for Toyoura sand

Parameter	Value	Reference
Unit weight, γ (kN/m^3)	15.78	Leung et al. 2000
Triaxial compression stiffness, E_{50}^{ref} (kN/m^2)	30×10^3	Deduced from Yamashita et al. 2000
Primary oedometer stiffness, E_{oed}^{ref}(kN/m^2)	24×10^3	Deduced from measured E_{50}^{ref}
Unloading/reloading stiffness, E_{ur}^{ref} (kN/m^2)	99×10^3	Deduced from measured E_{50}^{ref}
Effective friction angle, ϕ'(°)	43	Ong et al. 2006 and Leung et al. 2000
Dilatancy angle, ψ (°)	15	Bolton and Powrie 1986
K_0 value for normal consolidation, K_0^{nc}	0.318	Deduced from ϕ'value
Poisson's ratio, (ν)	0.3	
Reference stress for stiffness, p^{ref} (kN/m^2)	100	

Table 3.3. Pile properties

Parameter	Value
Bending rigidity (EI)	2.2×10^5 kN. m^2
Diameter	0.6 m
Length	12.5 m

3.2.3. FE modeling of centrifuge test

As mentioned in the previous section, PLAXIS 3D program was employed to model the centrifuge test in prototype scale, Figure 3.1 and 3.2 Only one half of the problem was simulated due to symmerty of loading and geometry. The size of the mesh was taken as (27 meter × 10 meter × 12.5 meter) in X-axis, Y-axis and Z-axis, respectively. The vertical sides of the model were restrained against to the horizontal movement, while the bottom side was restrained in all directions. The top side was free to move in any direction. The soil was simulated using 10-node element. The pile was simulated as an

embedded beam consists of beam elements which is 3-node line element, the interaction between the pile foot and pile skin and the surrounding soil was described as special interface element. The wall was modelled as 6-node triangular plate element. A 12-node interface element was used to to describe the actual interaction between the soil and the wall. The elements and interactions are described with more details in PLAXIS 3D Reference Manual V20. Medium type mesh was adopt in the anaylsis. The default setting of mesh refinements was used to refine the soil around the elements. The mesh consisted from 7017 soil element and 12770 node (Figure 3.4).

The numerical modelling procedure of centrifuge test was as following:

1. Initial phase: the automatically generated stage by PLAXIS to initiate the in-situ stresses with zero displacement using $K_0 = 1\text{-}\sin\phi$.
2. Activate the retaining wall and the pile.
3. Excavate the top 1.2 m of soil .

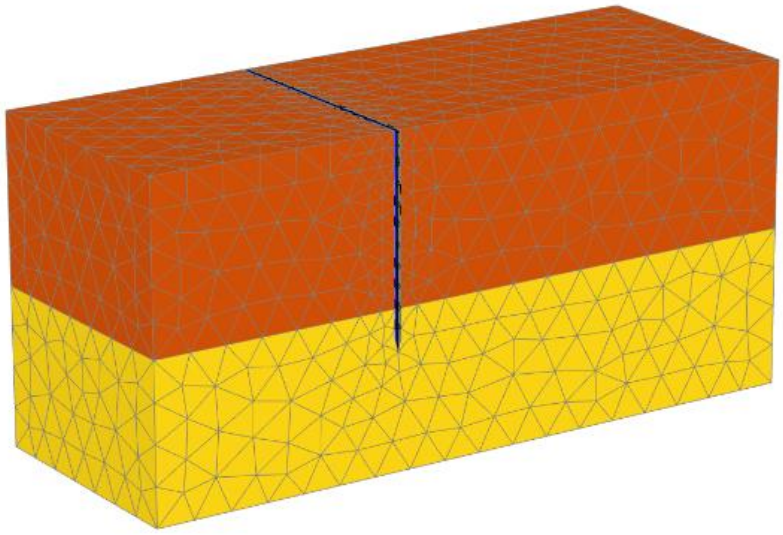

Figure 3.4. The used FE mesh in modelling the centrifuge test.

3.2.4. Comparsion between the computed and measured results

The computed and measured lateral deflection (LD) profile along the pile, as well as the generated bending moment (BM) owing to the adjacent excavation, are shown in Figures 3.5 and 3.6, respectively. It was noticed that the maximum LD occurs at the pile head in both measurements and the analysis results. The maximum deflection in measured results was 15 mm (1.5% from pile diameter) while the maximum deflection in computed results was 12 mm (1.2% from pile diameter), this difference decreases gradually with the depth. On the other hand, the induced BM for both computed and measured results was zero due to free head of pile. According to the computed results from numerical modelling; it was noticed that the bending moment increases gradually up to maximum value 87 kN.m at depth 6.5 m (52% from pile length), after 6.5 m it decreases gradually until reaching to the pile tip and becomes zero. The same trend was noticed for bending moment in measured results of centrifuge test. Generally, the computed bending moment shows a good agreement with the measured bending moments. Hence it can be adopted in the FE analysis later in this study.

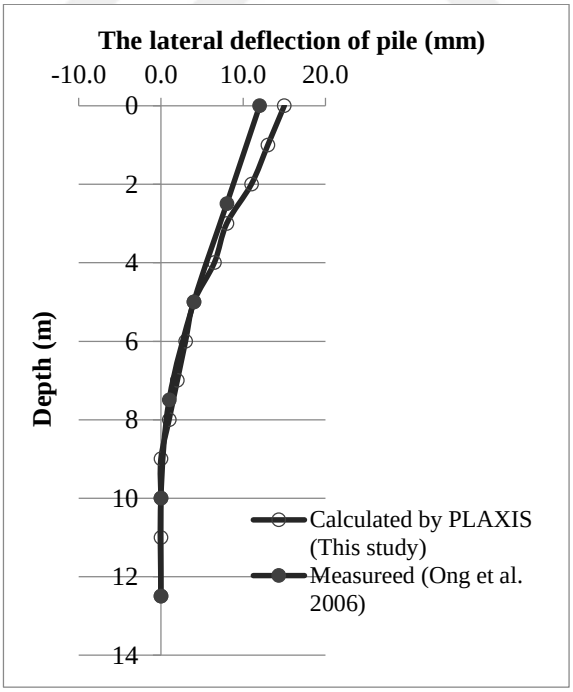

Figure 3.5. Comparison of computed and measured pile deflection owing to adjacent excavation.

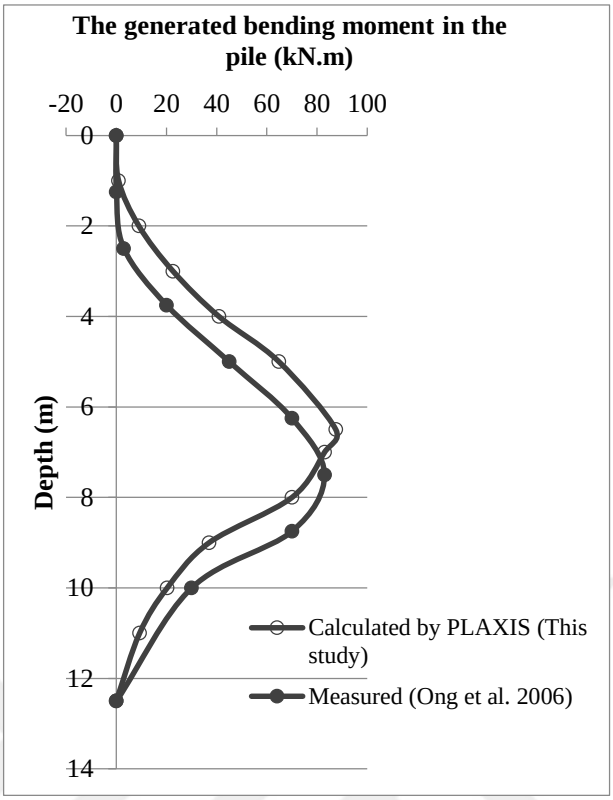

Figure 3.6. Comparison of computed and measured generated BM in pile owing to adjacent excavation.

3.3. Pile bearing capacity

3.3.1. Pile bearing capacity using PLAXIS 3D program

The parametric study aims to evaluate a loaded pile behavior owing to adjacent deep excavation in fully saturated sandy soil. Therefore, a pile load test was performed to calculate the pile bearing capacity using PLAXIS 3D program. A single bored concrete pile has a diameter of 1 meter, 20 meter length and elastic modulus of 30 GPa was loaded gradually with a point load (with increment of 500 kN). The model dimensions were taken as (40 meter × 40 meter × 40 meter) in X, Y and Z-axis, respectively. These dimensions were lager enough to avoid the boundary conditions effect. The medium type was adopt in the anaylsis. Figure 3.7 illustrates the finite element model which is used in the modelling of pile load test. The sandy soil was modelled using HS model,

the sand properties are given in Table 3.4. The pile was simulated as embedded beam with 3-node line element. Figure 3.8 shows the load-settlement curve. The pile ultimate capacity was determined using the settlement-based failure criterion for large diameter piles proposed by Ng et al. (2001). In the equation below, the failure criterion is given:

$$\Delta_{ph,max} \cong 0.045 d_p + \frac{1}{2}\frac{P_h L_p}{A_p E_p} \tag{3.1}$$

where:

$\Delta_{ph,max}$: maximum pile head settlement at the pile ultimate capacity

d_p : diameter of pile

P_h : applied load on pile

L_p : pile length

A_p : pile area

E_p : elastic modulus of pile

The ultimate bearing capacity was around 5000 kN based on this criterion, and the working load was calculated to be 1600 kN using a factor of safety of 3.

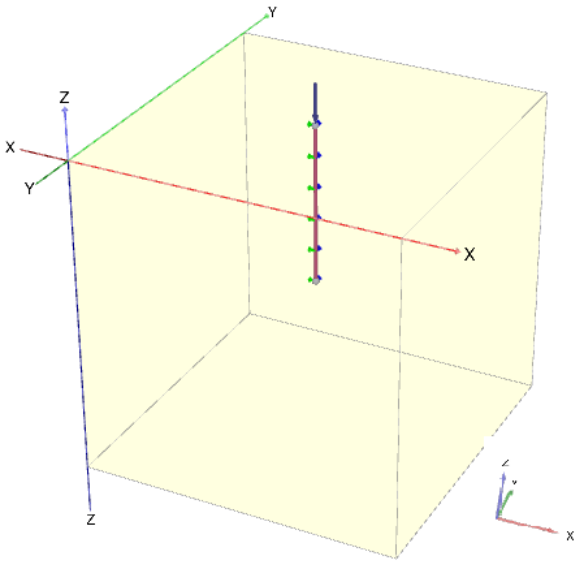

Figure 3.7. The finite element model which used in modelling of pile load test.

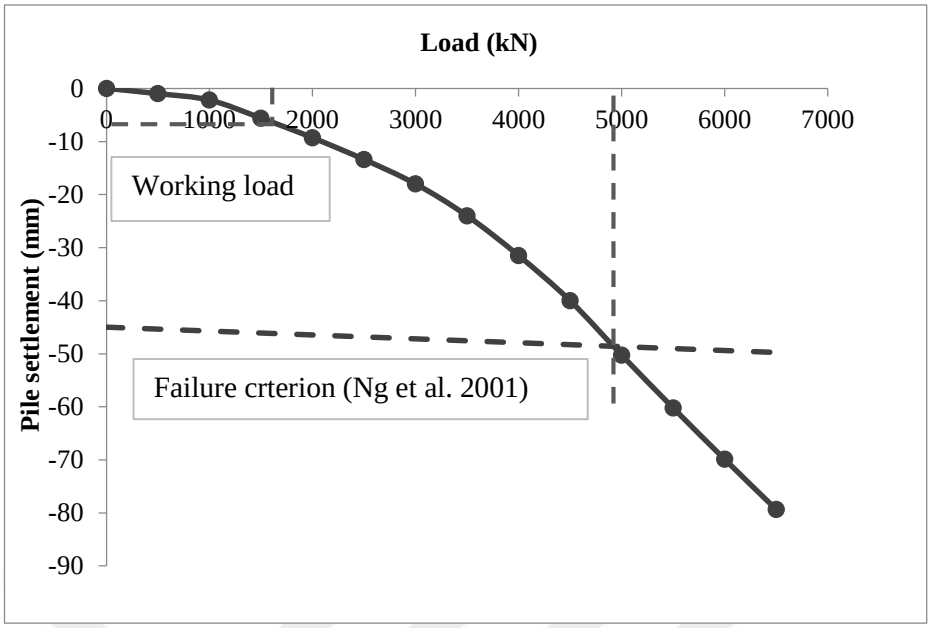

Figure 3.8. Load-settlement curve computed by PLAXIS 3D program.

3.3.2. Pile bearing capacity by empricial method

The following parameters will be used to calculate the pile bearing capacity; diameter of pile (d) = 1 meter, length of pile (L) = 20 meter, saturated unit weight (γ_{sat}) = 19 kN/m^3, friction angle of the sand (ϕ) = 43.2^0.

End bearing capacity of pile (Q_p):

Meyerhof method will be used to compute the value of Q_p for sand as follows:

$$Q_p = A_p \times q_p \leq Q_L \tag{3.2}$$

$A_p = \frac{\pi}{4} \times d^2$, $q_p = q' \times N_q^*$, $Q_L = 0.5 \times A_p \times P_a \times N_q^* \times \tan\phi$

So, $Q_p = A_p \times q' * N_q^* \leq 0.5 \times A_p \times P_a \times N_q^* \times \tan\phi$

where:

Q_p : pile end bearing load (kN)

A_p : cross sectional of pile area (m^2)

q' : effective vertical stress at the level of the pile end (kN/m^2)

N_q^*: Factor of load capacity (only dependent on ϕ- value (Das 2011))

P_a : atmospheric pressure = 100 kN/m^2

Q_L : Limiting value for point resistance (kN)

ϕ : friction angle of the sand

Skin resistance of pile (Q_s):

$$Q_s = \mathrm{P} \times \Sigma\, f_i \times L_i \tag{3.3}$$

P = π × D , $f_i = \mu_s \times$ N (where: μ_s = tan(δ) = tan(0.8ϕ) and N = $\sigma'_{v,av} \times$ K)

where:

P : pile perimeter (m), D : pile diameter (m), f_i : unit friction resistance at any depth (kN/m^2)

L_i : depth of each soil layer (m)

μ_s : friction coefficient between soil and pile, tan(δ) = tan(0.8ϕ)

N : horizontal stress from the soil to the pile, $\sigma'_v \times$ K (kN/m^2)

K : effective earth pressure coefficient = 1-sin(ϕ) or = 0.5 + 0.008 D_r (D_r is the relative density of soil (%))

Note that it was needed to draw the vertical effective stress along the pile to calculate the $\sigma'_{v,av}$ for each layer, but the stress will linearly increase to a depth of (15D), after which the stress will be constant (only for sandy soil), as shown in Figure 3.9.

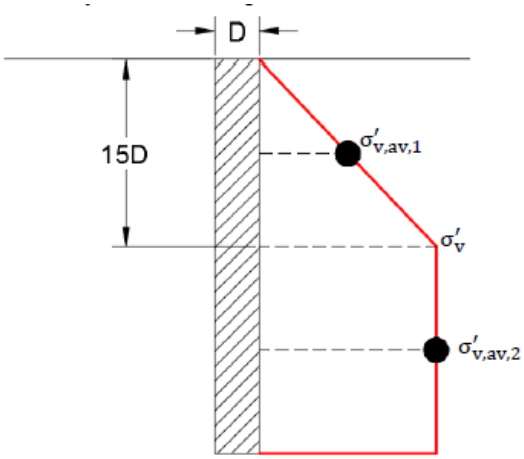

Figure 3.9. Stress distribution along the pile (Das 2011).

Hence,

$Q_p = (\frac{\pi}{4} \times (1)^2) \times (135.9) \times 130 = 17676$ kN $\leq 0.5 \times \frac{\pi}{4} \times (1)^2 \times 100 \times 130 \times \tan(43.2) = 4794$ kN

$Q_s = P \times \Sigma f_i \times L_i = P \times \Sigma \tan(0.8\phi_i) \times \sigma'_{v,av,i} \times K_i \times L_i$ (For each sand layer)

$Q_s = \pi \times 1 \times [\tan(0.8 \times 43.2) \times (1-\sin(43.2))] \times [(15 \times (135.9/2)) + (5 \times 135.9)] = 1160.27$ kN

$Q_{ult} = Q_p + Q_s = 4794 + 1160.27 = 5954$ kN

$Q_{all} = \frac{Q_{ult}}{F.S} = \frac{5954}{3} = 1984$ kN

So by using the empricial methods, the allowable load with F.S of 3 is 1984 kN. It was noticed that the pile bearing capacity calculated from empricial methods was a little larger than the bearing capacity calculated from finite element analysis, so the working load of 1600 kN will be taken in the numerical anaylsis.

3.4. Finite element model properties used in the anaylsis

3.4.1. Properties of finite element model and boundary conditions

In order to carry out the parametric study a typical finite element model was adopted (Figure 3.10). The properties of the model were kept as a constant and the variation effect of a certain factor will be investigated. Figure 3.11 shows the models that used in the anaylsis with different cases of H_e/L_p. The ratio of H_e/L_p= 0.5, 1 and 1.5 represent the excavation above, at and below the pile toe level, respectively. The ratio of wall penetration depth to depth of excavation was 0.5 in each anaylsis case (Hsiung, 2009; Ng at al., 2012). The excavation depth was equal to 10, 20 and 30 in the case of H_e/L_p= 0.5, 1 and 1.5, respectively. The pile length was kept as a constant, equal to 20 m. The model which has the ratio of H_e/L_p= 1 represents the typical model.

The model dimensions were taken as (50 meter × 20 meter × 70 meter) in X, Y and Z-axis, respectively. These dimensions were larger enough to avoid the boundary conditions effect. The boundary conditions of the model were the the same that in the modelling of centrifuge test. Medium type mesh was adopt in the anaylsis. The default setting of mesh refinements was used to refine the soil around the elements. The mesh consisted of 7102 soil element and 13532 node. Figure 3.12 illustrates the mesh utilized in the analysis. In this study, the sand properties were adopted from the study of Ünsever (2015). The sand was simulated using Hardening soil model (HS). The sand properties utilized in the analysis are mentioned in Table 3.4. The ground water table was assumed at the ground surface. The struts were spaced 2.5 meter and 10 meter in vertical and horizontal directions, respectively. The diaphragm wall and strut parameters utilized in the analysis are shown in Table 3.5 and 3.6, respectively. A single bored concrete pile with a diameter of 1 meter and a length of 20 meter was placed at 3 m (center to center) from the diaphragm wall in the model. The working load of 1600 kN was applied on the head of pile. The pile properties utilized in the analysis are mentioned in Table 3.7. The pile was modelled as an embedded beam.

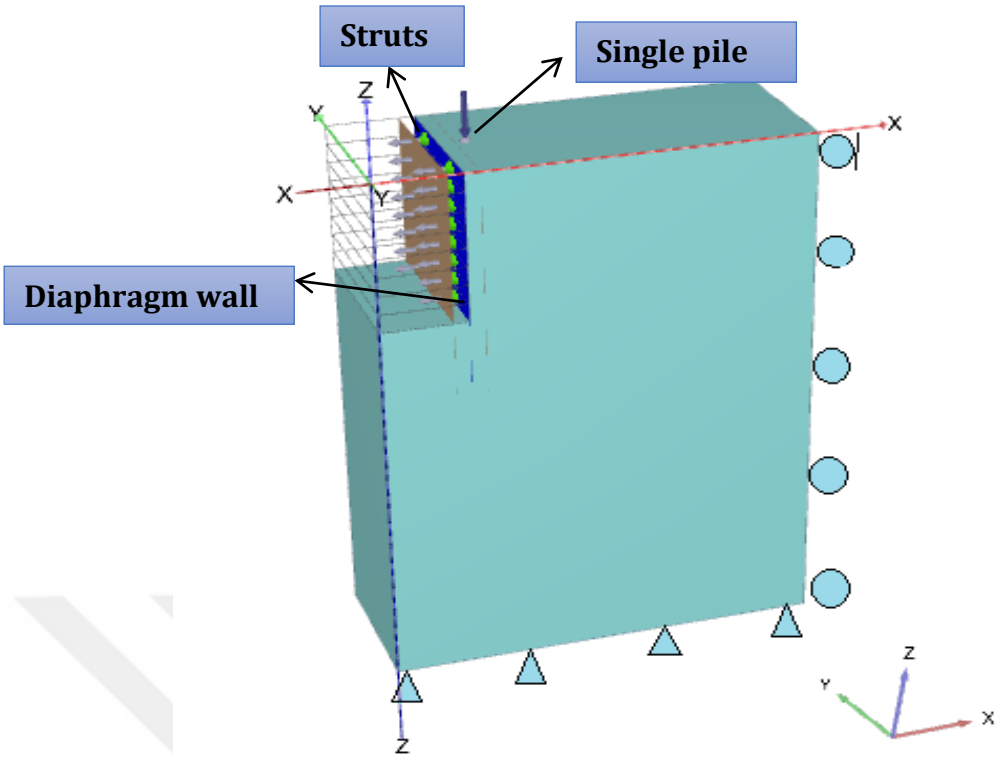

(a)

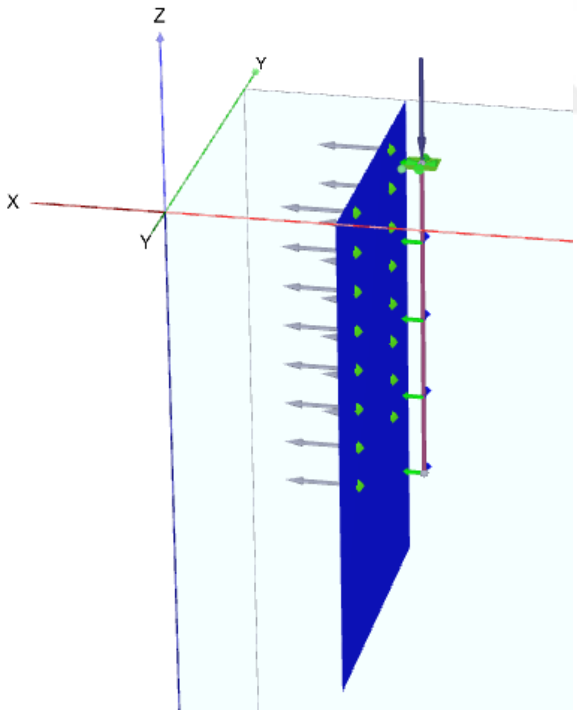

(b)

Figure 3.10. Typical used finite element model (a) Bounary conditions (b) Structural elements .

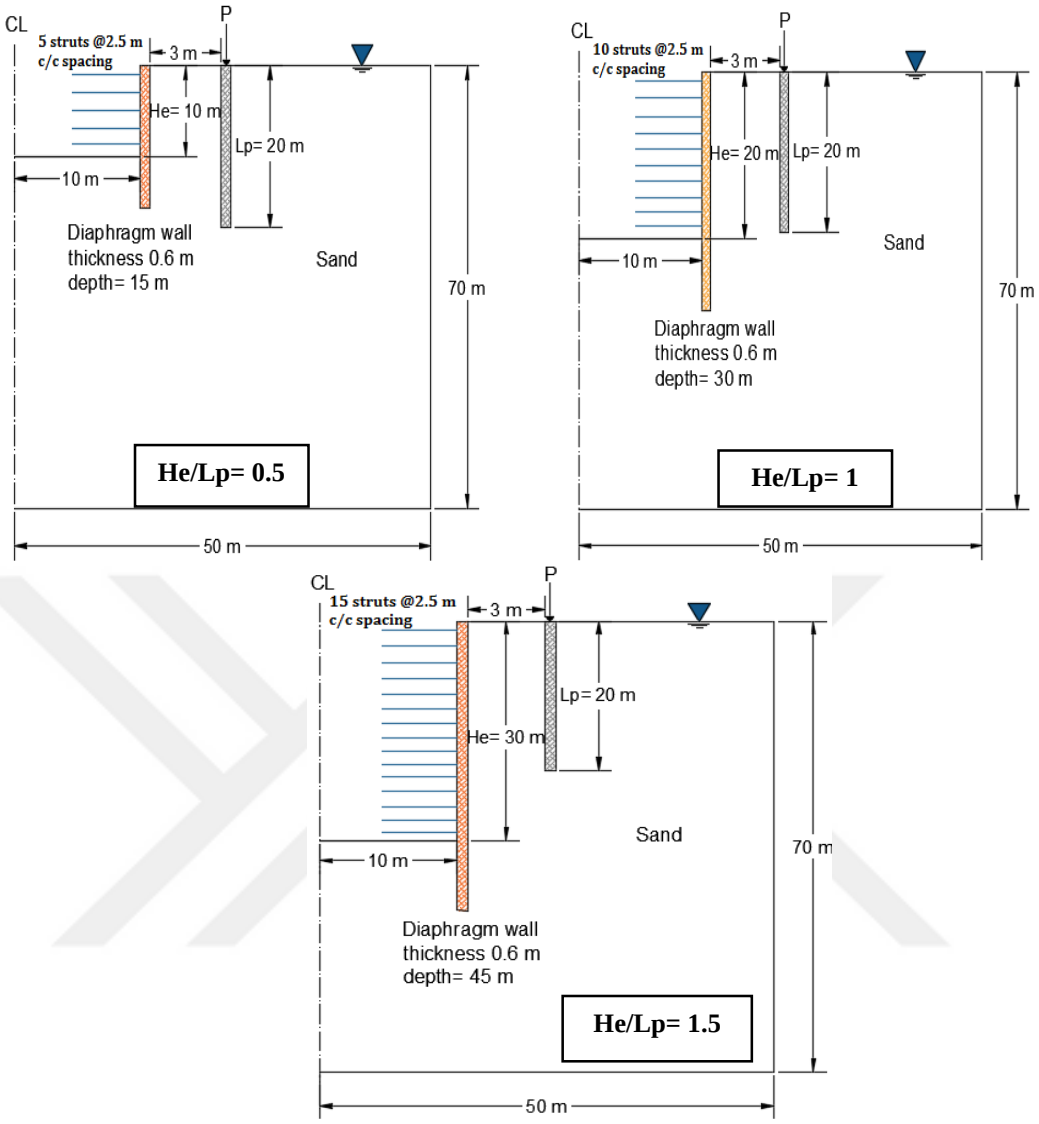

(a)

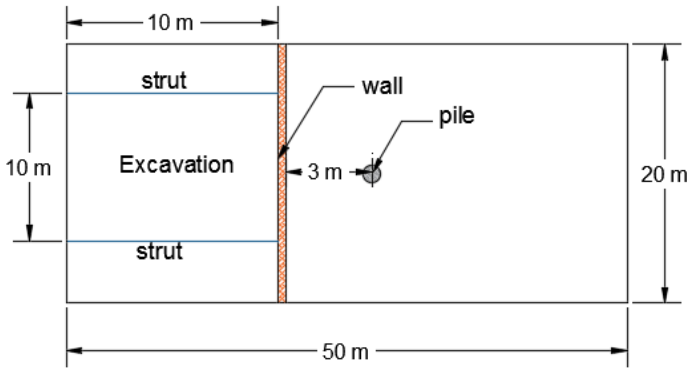

(b)

Figure 3.11: (a) Cross section of model for the three cases of H_e/L_p (b) Plane view.

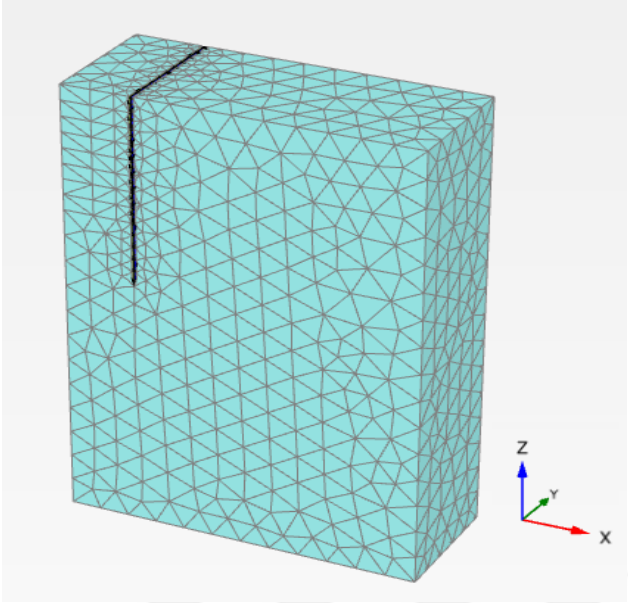

Figure 3.12. Finite element mesh.

Table 3.4. Sandy soil properties (Ünsever, 2015)

Parameter	Value
Dry Unit weight, γ_d (kN/m^3)	14.52
Saturated unit weight, γ_{sat} (kN/m^3)	19
Initial void ratio, $e_{initial}$	0.83
Triaxial compression stiffness, E_{50}^{ref} (kN/m^2)	29.56×10^3
Primary oedometer stiffness, E_{oed}^{ref} (kN/m^2)	24.65×10^3
Unloading/reloading stiffness, E_{ur}^{ref} (kN/m^2)	99.59×10^3
Effective friction angle, ϕ'(°)	43
Dilatancy angle, ψ (°)	15.8
K_0 value for normal consolidation, K_0^{nc}	0.318
Poisson's ratio, (ν)	0.19
Reference stress for stiffness, p^{ref} (kN/m^2)	100
Cohesion (kN/m^2)	0.1
Interface reduction factor	0.75

Table 3.5. Diaphragm wall (plate element) parameters

Parameter	Value
Unit weight , γ (kN/m^3)	25
Thickness (m)	0.6
Young's Modulus, E (GPa)	30
Poisson's ratio, (ν)	0.3

Table 3.6. Strut (fixed end anchor) parameters

Type	Axial rigidity	Area (m^2) ×10^{-4}	Young's Modulus (GPa)
H 150×75×5×7 steel	374.85×10^3	17.85	210

Table 3.7. Embedded pile parameters

Parameter	Value
Unit weight , γ (kN/m^3)	25
Young's Modulus, E (GPa)	30
Pile diameter, d_p (m)	1
Pile length, L_p (m)	20
Skin resistance	Layer dependent
Maximum skin resistance, T_{max} $(kPa)^a$	380
Maximum base resistance, B_{max} $(kPa)^b$	1598

^{a,b} Computed by empirical method

3.4.2. Finite element modelling procedure of the typical model

The finite element modelling procedure can be summarized as follows:

- ✓ ***Soil mode*:** The geometry model was created, and the soil stratigraphy was defined. In addition, the data set of soil layer was created. The soil properties window includes: choosing the constitutive model, picking up the material type (drained or undrained) and entering the parameters of the soil (i.e. density, strength parameters, stiffness, Poisson's ratio and interface).
- ✓ ***Structure mode*:** All the structural elements were generated such as, the pile, the loads, the diaphragm wall, the struts and excavation levels. Then the structural

properties of each element should be defined. The pile and wall properties window includes: type of behaviour, normal stiffness, flexural rigidity, unit weight, Poisson's ratio. The strut properties window includes: type of behaviour, normal stiffness and spacing out-of-plane.

- ✓ ***Mesh Mode*:** The mesh was established.
- ✓ ***Flow conditions*:** The groundwater level was defined.
- ✓ ***Staged construction:*** The construction stages were defined in this step. In reality, constructing an excavation might be a multi-phased procedure. First, the single pile was driven to the desired depth and then the pile was loaded to the maximum allowable load. After that, the wall was built to the appropriate depth. Then additional excavating was done to make space for the struts to be installed. The soil is then gradually excavated until the excavation reaches its final depth (formation level). Special measures are usually taken to keep the water out of the excavation. In PLAXIS, these processes can be modelled with "Staged construction" calculation option. This tool enables the activation or deactivation of volume, weight, stiffness, and strength of the selected components of the finite element model. The following is a summary of the numerical analysis modelling procedure for a typical model (i.e., H_e/L_p= 1):

- ***Stage 0 Initial phase:*** *It* is an automatically generated stage by PLAXIS to initiate the initial stresses using K_0= 1-sinϕ' procedure.
- ***Stage 1 Pile construction*:** In this stage a pile with length of 20 m is constructed (activated).
- ***Stage 2 Applying the load:*** A working load of 1600 kN was applied to the head of the pile.
- ***Stage 3 Wall construction*:** in this stage the diaphragm wall was installed as cast-in-situ pile (activated).
- ***Stage 4 Excavation***: The first 2.5 m depth of soil are excavated (deactivated).
- ***Stage 5 Strut installation***: First strut installation: The first level of struts were installed in this stage at 1.25 m depth from the ground surface.

  Then the Stage 4 and 5 will be repetitive until reaching the final depth of excavation, which is equal to 20 m.

4. RESULTS and DISCUSSION

4.1. Influence of excavation depth on pile response

In order to evaluate the effect of excavation depth on the pile behavior, situated at 3 m from the wall; three different cases of excavation depth to a constant pile length (H_e/L_p) were studied. As mentioned in the previous section, the ratio of H_e/L_p= 0.5, 1 and 1.5 represent the excavation above, at and below the pile toe level, respectively. The pile length was kept as a constant (equal to 20 m) during these analyses.

4.1.1. Ground surface settlement (GSS) and lateral movement in free-field condition

To evaluate the effect of excavation depth (H_e) on ground settlement behind the wall a free-field condition without pile beside the excavation was studied in three different cases of H_e/L_p. Figure 4.1 shows the GSS behind the diaphragm wall owing to the excavation after reaching to the final depth for all the three cases. It was noticed that the GSS behavior behind the wall affected by H_e significantly and the settlement curve become wider as H_e increases. For the case of H_e/L_p= 0.5 the settlement decreases with increasing distance behind the wall (0≤ X ≤15 m), then it becomes constant after 15 m distance (1.5H_e). The settlement profile for case of H_e/L_p= 1 and 1.5 approximately have a spandrel type and the settlement increases with increasing distance (this specific distance, X= 5 m and 10 m for cases H_e/L_p= 1 and 1.5, respectively). After this distance the settlement decreases and becomes constant. The maximum settlement was 9.5, 13 and 22 mm for the cases of H_e/L_p= 0.5, 1 and 1.5, respectively. The reason for the GSS even at a relatively far distance from the wall can be attributed to the granular sandy soil behaviour.

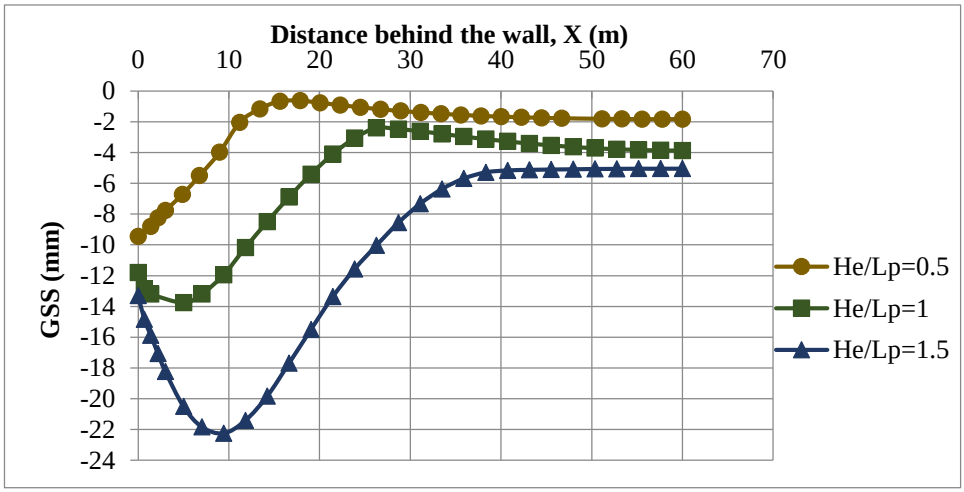

Figure 4.1. GSS behind the diaphragm wall owing to the excavation for three cases of H_e/L_p.

Figure 4.2 illustrates the lateral movement of the ground surface owing to the excavation after reaching to the final excavation depth for the three cases of H_e/L_p in free-field condition. It was noticed that the ground movement increases significantly as the excavation depth increases and it decreases as the distance from the wall decreases. This ground lateral movement leads to stress release which lead to produce lateral deflection (LD) and bending moment (BM) on the pile as will be discussed in the following sections.

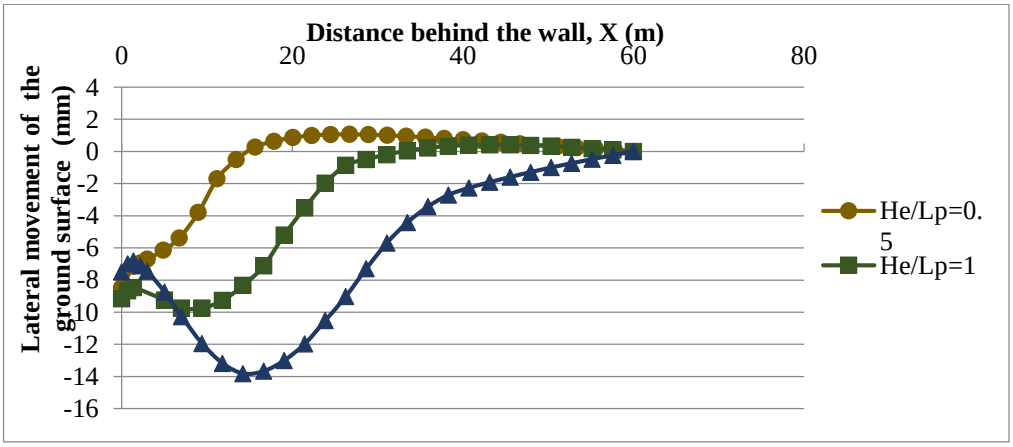

Figure 4.2. Lateral movement of the ground surface owing to the excavation for three cases of H_e/L_p in free-field condition.

4.1.2. The lateral deflection of diaphragm wall due to the excavation

Figure 4.3 illustrates the lateral deflection of wall for three cases of H_e/L_p. In the case of H_e/L_p= 0.5 the wall deflects towards excavation with maximum value at the wall head (8.6 mm) then it decreases slightly with the increase of wall depth. In contrast, in the case of the wall deflection H_e/L_p= 1 and 1.5 , the curve increases to the mid-depth of the wall and then it begins to decrease. This can be attributed to the struts that support the wall and push it towards the soil. The wall deflection was highest in the case of the highest excavation depth as expected. The deflection at the wall head are 9.3 and 8.2 mm, where the maximum LD of the wall is 16.7 mm and 32.4 mm at depth of 12 m (40% from wall depth) and 20.6 m (46% from wall depth) for the case of H_e/L_p= 1 and 1.5, respectively.

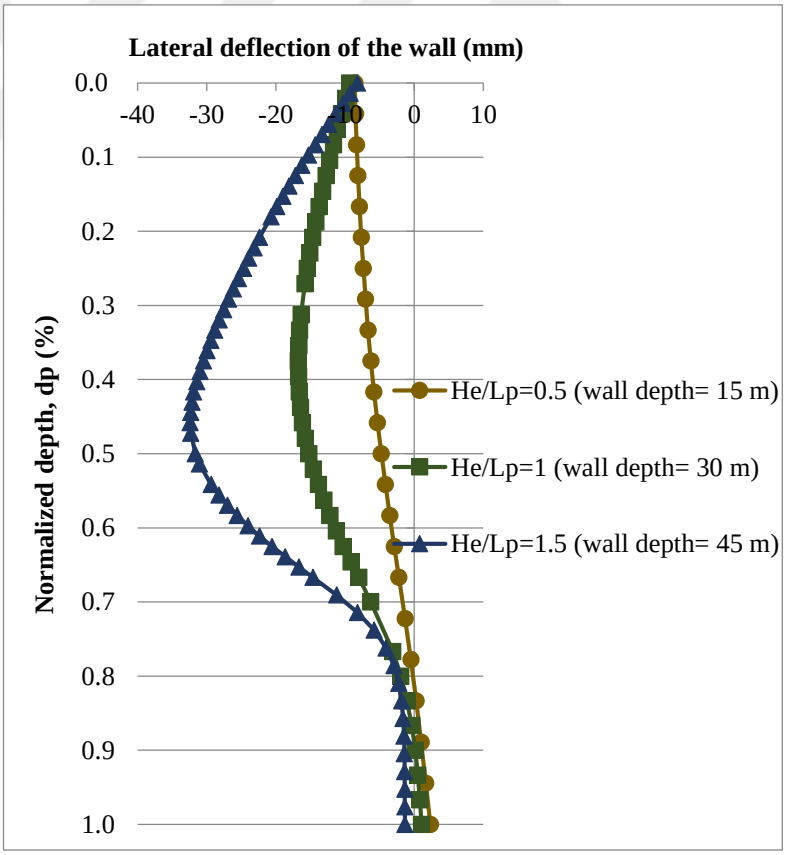

Figure 4.3. Lateral deflection of the wall for each H_e/L_p cases.

4.1.3. The pile settlement due to the excavation

Figure 4.4 illustrates the loaded pile settlement along the pile length owing to the excavation in the three cases of H_e/L_p. The pile settlement increases as the excavation depth increases, according to the results. Moreover, the settlement is constant along the pile axis. The maximum pile settlement is 10, 20 and 37 mm (i.e., 1%, 2% and 3.7% from pile diameter d_p) for the case of H_e/L_p = 0.5, 1 and 1.5, respectively. By comparing these values with the settlement of pile at the working load (6 mm "0.6%d_p"), it can be noticed that for both of the three case the pile settlement exceeds the allowable limit of pile settlement. This may be produce a potential serviceability problem for piles foundations due to adjacent excavation.

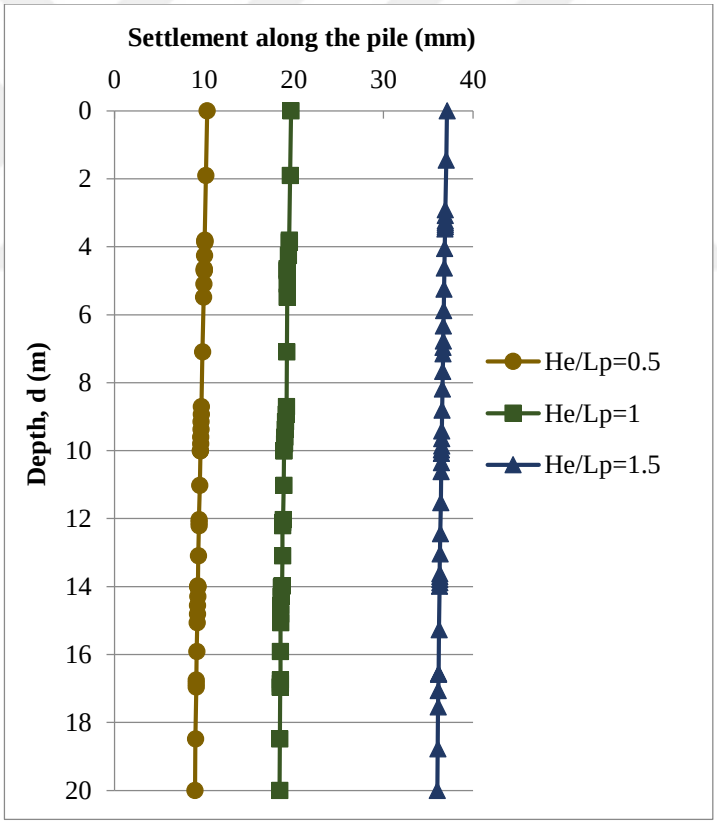

Figure 4.4. Settlement of the loaded pile along the pile length owing to the excavation for three cases of H_e/L_p.

4.1.4. The pile lateral deflection due to the excavation

Figure 4.5 illustrates the pile lateral deflection profile owing to the excavation in three cases of H_e/L_p. The vertical axis of the graph was normalized by pile length for comparison reason with another studies as will be explained later. The negative values indicate that the pile is moving closer to excavation. As in the figure, it can be observed that the pile was displaced in the direction of the excavation in the three cases of H_e/L_p as expected, because the excavation lead to stress release and displacement of soil towards excavation. In the case of H_e/L_p= 0.5 which means the pile toe situated below the final level of excavation (H_e), the results appear that the the pile head exposed to maximum deflection because the free head of pile and the upper portion of the pile (until 11 m of pile length) deflects towards the excavation side while the lower portion stays almost stable. This is because of the embedded part of the pile with respect to the final level of excavation, which provides the pile stabilization. In the second case ($H_e/L_p = 1$) which means the pile toe situated at the same of H_e; the results appears that both the pile head and toe displace to excavation side. The deflection increases from the pile head until 11 m (55% from pile length L_p) with a maximum value of 13 mm (1.3%d_p) along the pile length then it begins to decrease. In the third case ($H_e/L_p = 1.5$), which means the pile toe situated above the H_e; it appears that both the pile head and the toe moves towards the excavation side. But the pile toe deflection (equal to 24 mm) is larger than the pile head deflection. This is because of the relatively larger H_e.

The centrifuge test results conducted by Leung et al. (2000) (H_e of 4.5 m with no struts and pile length of 12.5 m) are given in Figure 4.5 for comparison purposes. Because the conditions are similar, the pile lateral deflection profile in that study behaves similarly to the lateral deflection profile in the case of H_e/L_p=0.5, as shown in the figure.

Figure 4.6.a, b and c illustrates the lateral deflection of the pile at different excavation stages in the three cases of H_e/L_p. According to the results, the LD of the pile increases

with the increasing of h in the three cases of H_e/L_p. The upper portion of the pile was deflected more than the lower portion in all excavation stages at H_e/L_p= 0.5 (Figure 4.6.a). Moreover, throughout the excavation process, the pile was rotated counter-clockwise around an axis perpendicular to the plane of the paper. The transition point was about at 9.6 m depth (48% of pile length L_p). When the excavation is finished (at h=10 m) the maximum LD was at the pile head with a value of 8.5 mm (0.85% of pile diameter d_p). Similarly, in the case of H_e/L_p= 1 (Figure 4.6.b), the results show that both the pile head and the pile toe moves to the excavation site but the pile head deflection was higher than the pile toe deflection except in the final excavation depth (h=20 m), which the deflection behavior was different relatively comparing to the previous stages. In the case of H_e/L_p= 1.5 (Figure 4.6.c), the pile deflected as the same way in case of H_e/L_p= 1, but in the final excavation stage (h= 30 m) the maximum deflection was at the pile toe with value of 23.6 mm (2.36%d_p).

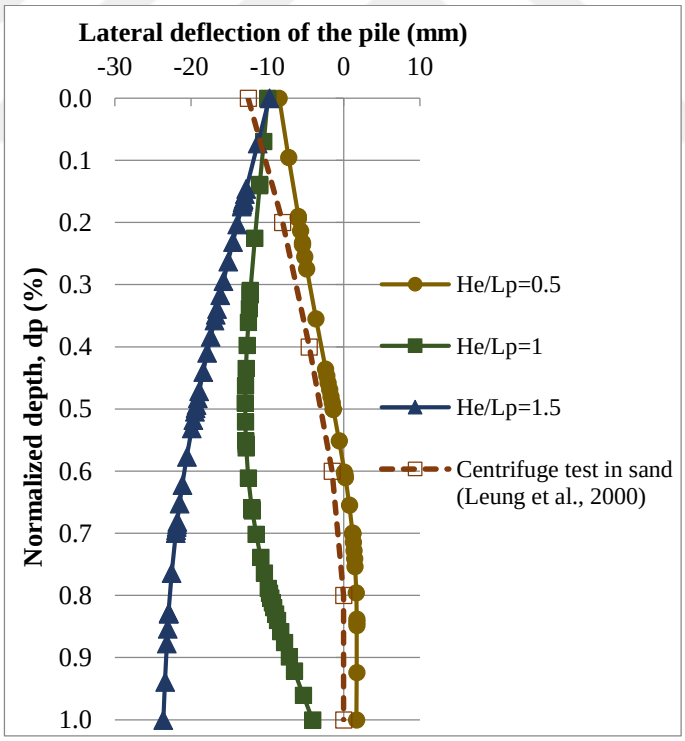

Figure 4.5. Lateral deflection of the pile owing to the excavation for three cases of H_e/L_p.

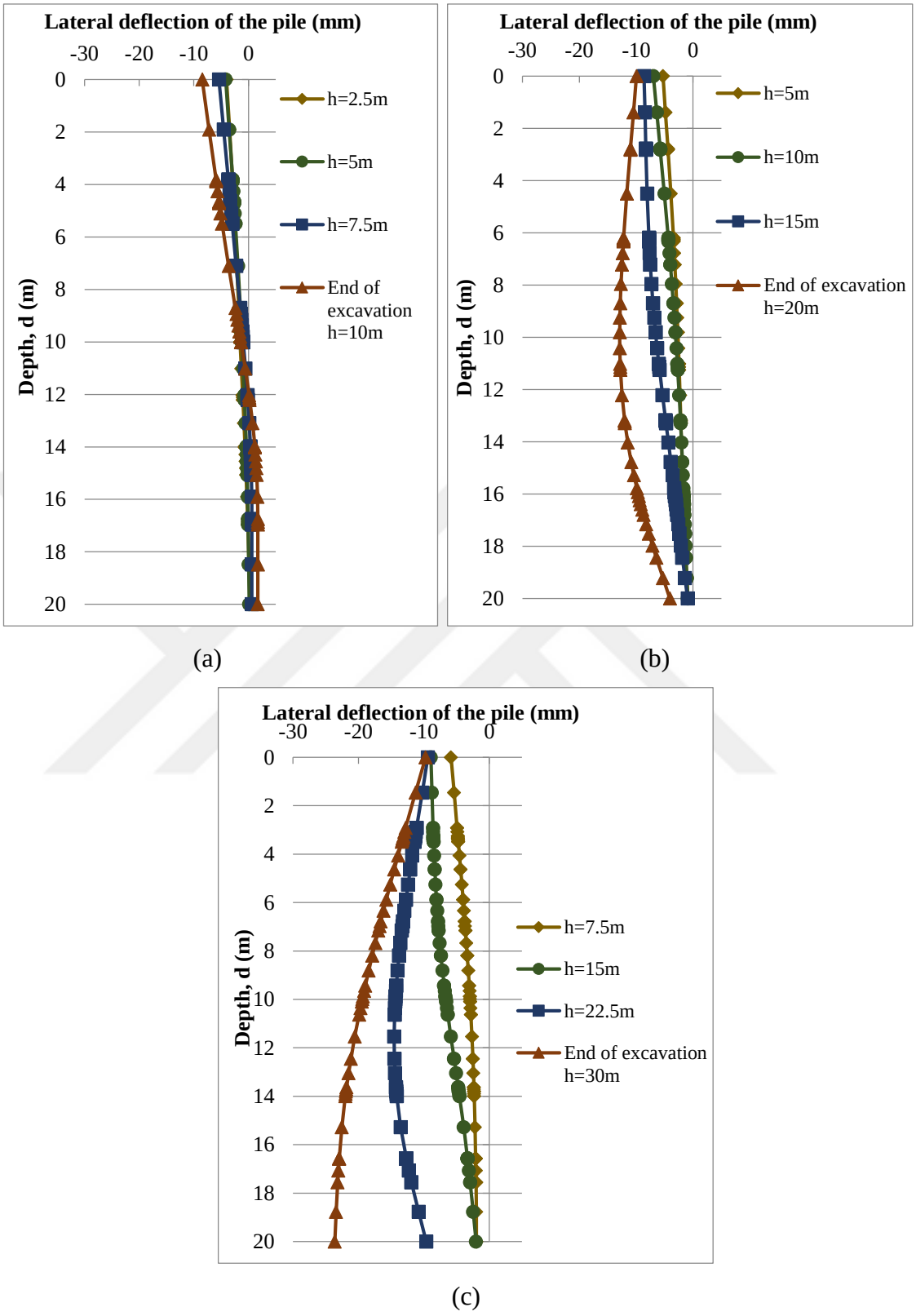

Figure 4.6. Lateral deflection of the pile at different excavation stages in three cases of H_e/L_p (a) H_e/L_p= 0.5 (b) H_e/L_p= 1 (c) H_e/L_p= 1.5.

4.1.5. The generated pile bending moment due to the excavation

Figure 4.7 illustrates the generated BM profile at the pile owing to the excavation in the three cases of H_e/L_p. The negative values mean that the pile is exposed to tensile stress along the pile shaft. Because of the free head of the pile, the induced BM at the pile head is zero in all cases. From the figure, it can be seen that for the case of H_e/L_p = 0.5, the negative BM increases gradually at the upper portion of the pile (0≤ Z ≤ 8.75 m) then the moment becomes positive in the below portion and increases gradually, BM becomes zero at the pile toe. For the case of H_e/L_p = 1 and 1.5 it can seen that the pile shaft was exposed to negative BM, meaning that the pile shaft is under tensile stress. The case of H_e/L_p = 1 developed the highest bending moment because the pile toe was at the same level with H_e, while the case of H_e/L_p = 0.5 developed more bending moment with respect to the case of H_e/L_p = 1.5, because H_e/L_p = 0.5 experienced higher restraint from the surrounding soil. Hence, it can be concluded that the case of H_e/L_p = 1 generates the highest bending moment while the case of H_e/L_p = 1.5 generates the lowest bending moment.

Ng. et al. (2017) conducted a centrifuge test (H_e was 8 m with 2 levels of soft struts and pile length of 20 m) and the results are shown in Figure 4.7 for comparison. According to the figure, it can be noticed that the negative BM's generated at the ground surface and the upper portion of the pile (until 0.43L_p) but the lower portion exposed to positive bending moment. Also, it can be noticed that the pile has the same trend of BM profile in case of H_e/L_p = 0.5 that analyzed in this study but the values were larger especially at the ground surface and at the upper portion of the pile although the pile has a free head. This is may be attributed to two reason, firstly, the ground surface made rotation at the restraint level above the ground, as commented by Ng. et al. (2017). Secondly, The wall and the struts that used in the centrifuge test were soft enough to make high negative moments in the upper portion of the pile compared with the case of H_e/L_p = 0.5 that analyzed in this study. Another results from centrifuge test conducted by Leung et al. (2000) are showed in the same figure. From the figure it can be noticed that only

positive moment generated along the pile length with maximum value at about 0.6 of normalized pile length. Thus it can be said that the different conditions of each analysis and test actually lead to different results in generated BM profile of a pile.

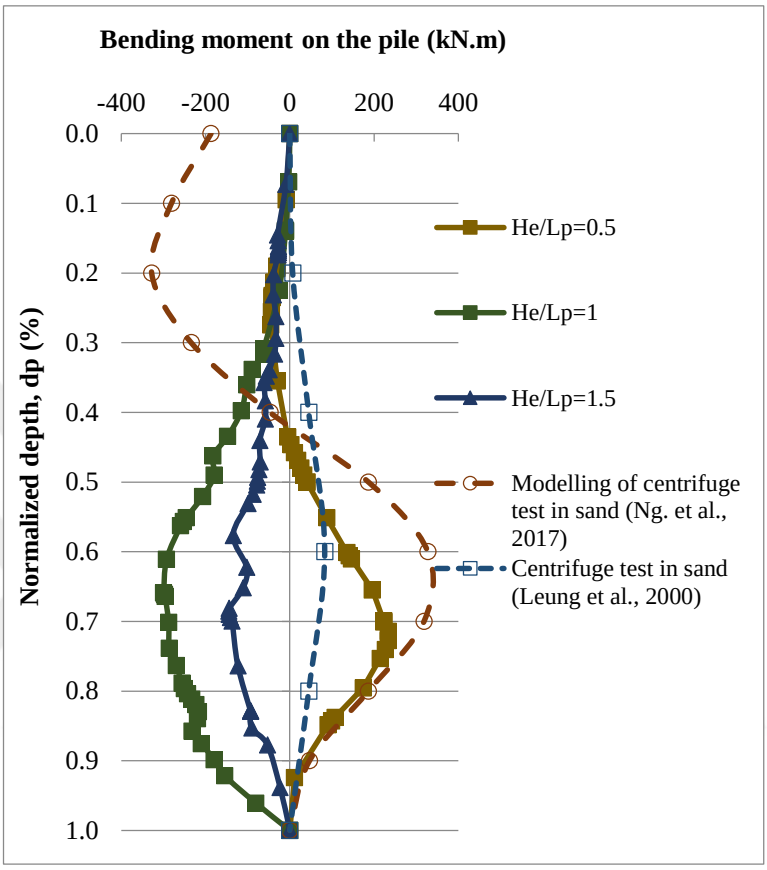

Figure 4.7. Bending moment on the pile owing to the excavation in three cases of H_e/L_p.

Figure 4.8.a, b and c illustrates the generated bending moment at different excavation stages in the three cases of H_e/L_p. Generally, it was noticed that the generated bending moment increases as the excavation proceeds in the three case of H_e/L_p. In H_e/L_p=0.5 case, the positive bending moment gradually increased in the lowest portion of the pile as the excavation proceeds. For the both case of H_e/L_p= 1 and 1.5, the bending moment turned gradually from positive to negative as the excavation proceeds. This is because of pile toe location with respect to the final excavation depth as discussed above.

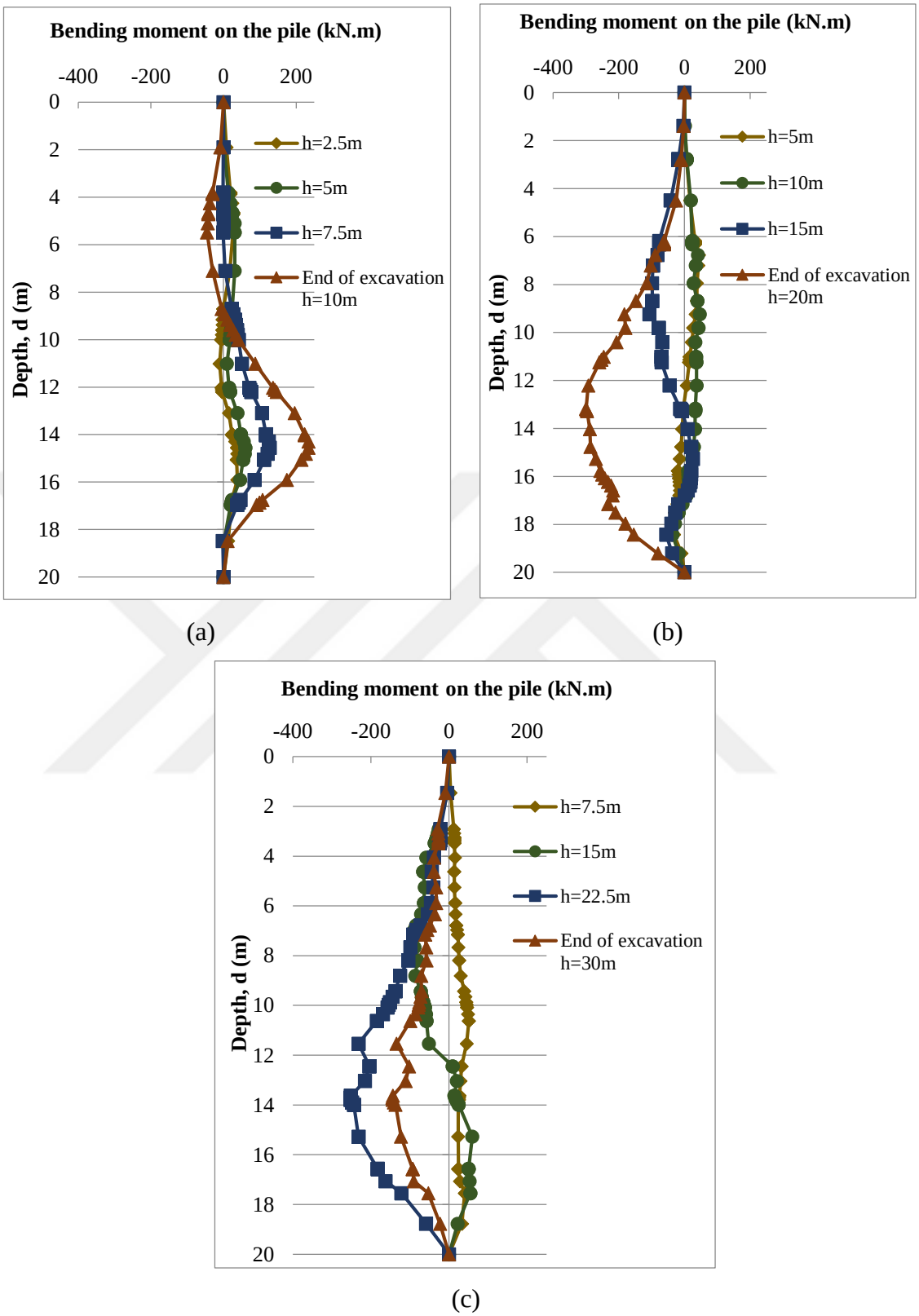

Figure 4.8. Bending moment on the pile at different excavation stages in the three cases of H_e/L_p (a) H_e/L_p= 0.5 (b) H_e/L_p= 1 (c) H_e/L_p= 1.5.

4.1.6. The distribution of axial load along the pile

Figure 4.9 illustrates the distribution of axial load along the pile shaft before and after the excavation in the three cases of H_e/L_p. Before the excavation, it can be noticed that the pile shaft and pile toe shared 62.5% and 37.5% of the working load, respectively. After the excavation, in the case of H_e/L_p = 0.5, the induced negative shaft resistance in the upper portion of the pile led to increase the axial load gradually to 1929 kN (20% increase from the applied working load), while the axial load decreases owing to the induced positive shaft resistance in the lower part of the pile. In case of H_e/L_p = 1, the axial load increase slightly to 1780 kN and then it decreases in the lower portion of the pile owing to the induced positive shaft resistance. In case of H_e/L_p= 1.5, the axial load distribution profile is similar the axial load distribution profile before excavation. However, the ratio of transferred load by toe was higher than before excavation case. At the final level of excavation, about 42% of the applied load is carried by the pile shaft for both H_e/L_p= 0.5 and 1.5 cases, while this ratio reduced to 19% in case of H_e/L_p= 1. The location of the pile toe to H_e level is the reason of the decrement in the load carried by the pile shaft.

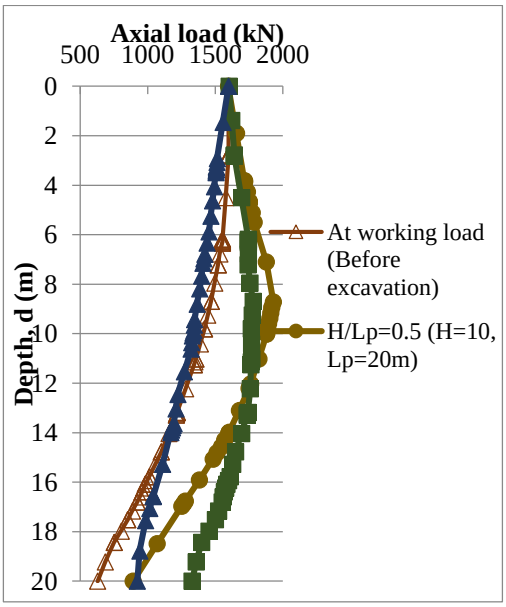

Figure 4.9. Axial load distribution along the pile shaft before and after excavation in three cases of H_e/L_p.

4.2. Influence of the distance from pile to excavation on pile response

In order to evaluate the effect of horizontal distance of the excavation site on pile behavior, six distances of 3, 5, 7, 9, 11 and 20 m (i.e., 15%, 25%, 35%, 45%, 55%, and 100% from the final excavation depth H_e) were examined. The final excavation depth and pile length were kept constant, equal to 20 m (H_e/L_p= 1). Figure 4.10 illustrates the lateral pile deflection distribution due to changing distances between the pile and the excavation area (X). It can be observed that the increasing of distance X lead to decreasing the lateral deflection of the pile as expected. The deflection profile totally changes from curve to a line as the distance increases. Also, it can be observed that the deflection of pile head decreases significantly when the distance equal to 20 m. Moreover, the pile toe deflection decreases as the distance increases.

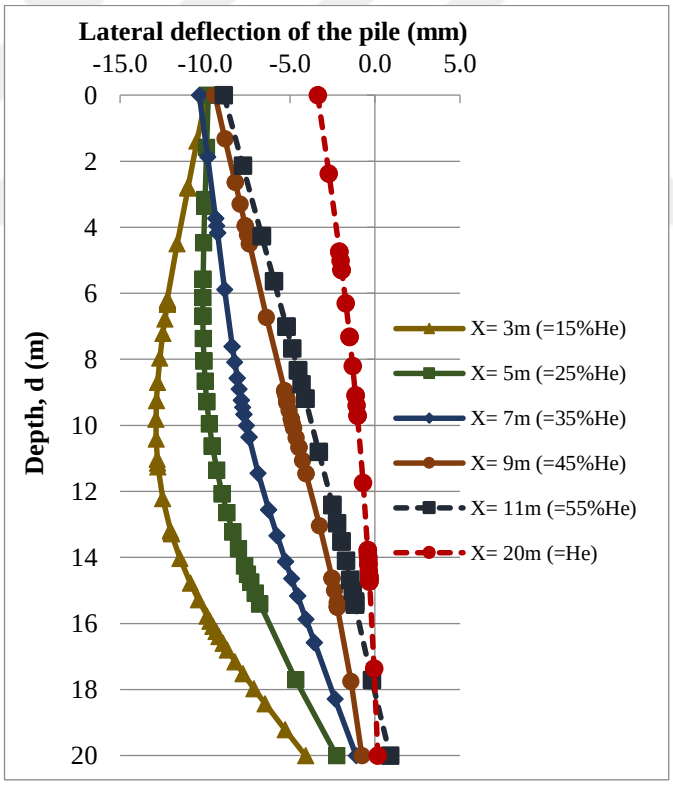

Figure 4.10. LD of the pile due to changing the distance from the pile to the excavation site.

Figure 4.11 illustrates the profile of the bending moment due to changing the distance (*X*). It can be observed that the increasing of the distance *X* leads to decreasing the BM significantly. In the first three cases (3, 5 and 7 m), the pile was exposed to negative BM. After 11 m distance, only positive BM induces in the pile with insignificant values. It can be said that, the induced bending moments on the pile are negligible after 9 m.

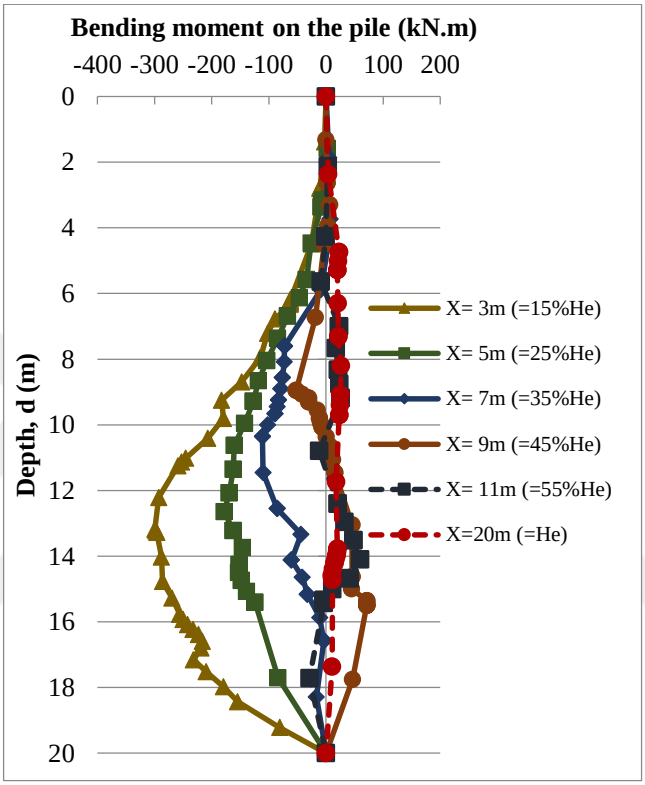

Figure 4.11. BM on the pile due to changing the distance from the pile to the excavation site.

Figure 4.12 illustrates the bending moment in pile in case of H_e/L_p= 1 at different distances of (X) with the progress of the excavation. After X=11 m distance between the pile and the excavation site, the negative moments induced on the pile are insignificant and positive bending moments are lower than 50 kN.m.

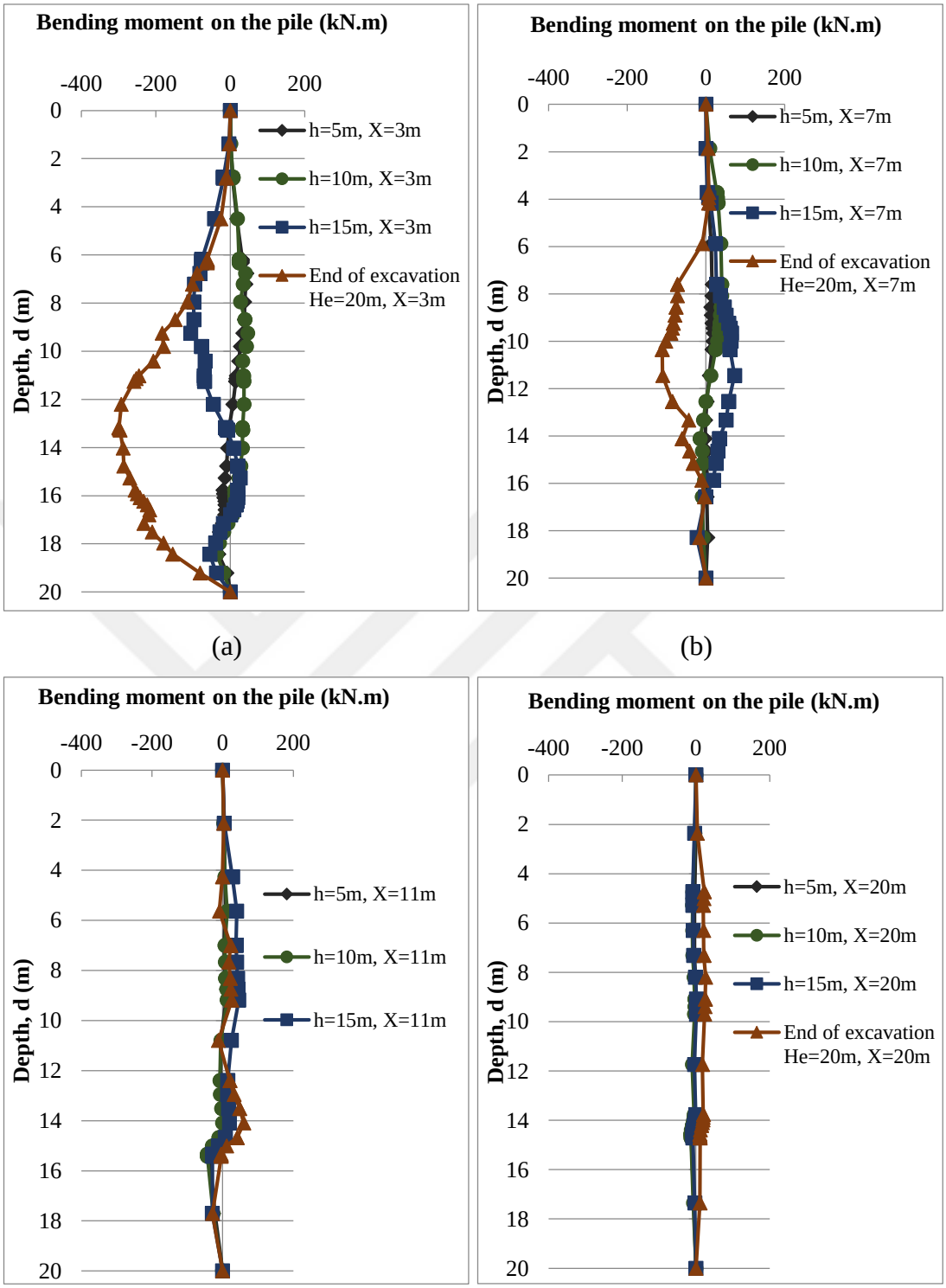

Figure 4.12. Bending moment on the pile in case of H_e/L_p= 1 at different distances of (X) with the progress of the excavation (a) X= 3 m (b) X= 7 m (c) X= 11 m (d) X= 20 m.

4.3. Influence of pile length on pile response

Three different lengths of 20, 30, and 40 m (i.e., Lp/He= 1, 1.5, and 2, respectively) were examined to evaluate the influence of pile length on the pile behavior. The excavation depth was fixed to 20 m depth. Figure 4.13 illustrates the lateral deflection of the pile due to changing the pile length. It can be noticed that the LD of pile was very similar for all three cases. Figure 4.14 illustrates the generated BM on the pile due to changing the pile length. It can be noticed that the differences are an insignificant between the three cases. Above portion of the pile induced negative BM and the below portion of the pile exposed to positive bending moment, approximately after 20 m from pile length, which is the excavation depth.

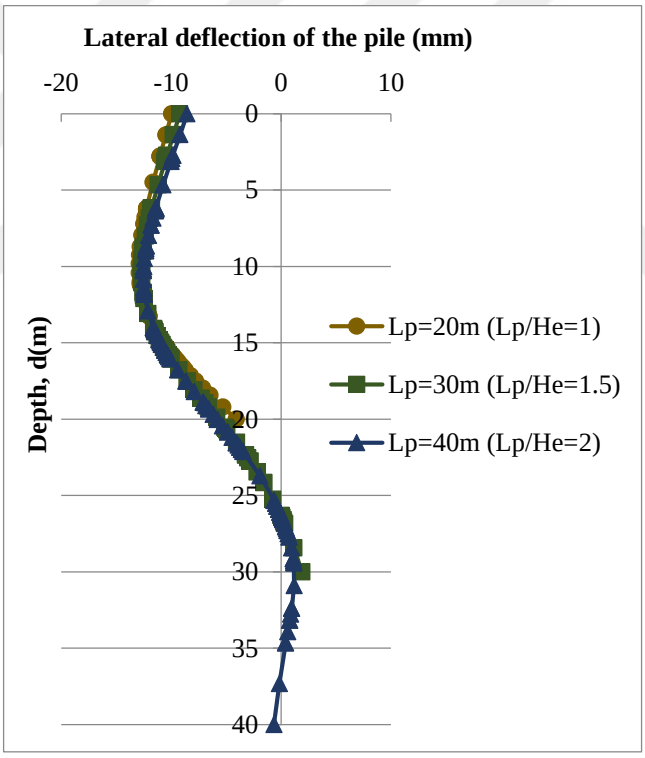

Figure 4.13. LD of the pile due to changing the pile length.

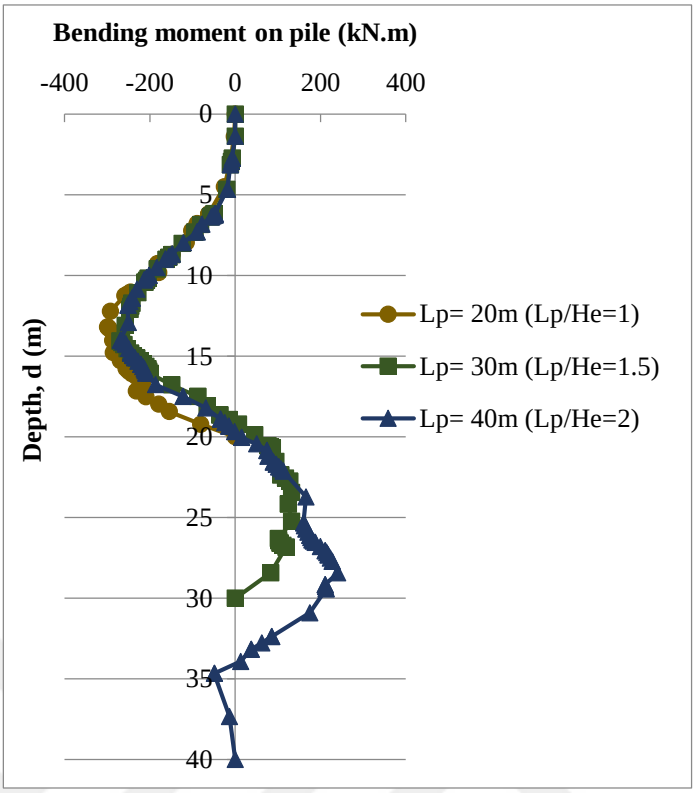

Figure 4.14. BM on the pile due to changing the pile length.

4.4. Influence of working load on the pile response

Figure 4.15 illustrates the axial load distribution along the pile shaft before and after the excavation at different factor of safety (F.O.S) in the case of H_e/L_p= 0.5. The value of F.S= 3.0, 2.5 and 2.0 corresponds to the working load of 1600, 2000 and 2500 kN, respectively. After excavation the transferred axial load along the pile shaft increases gradually with the ratio of 16%, 10% and 6.4% from the applied working load for F.S= 3, 2.5 and 2, respectively. Before excavation, pile shaft shared 35%, 44% and 52% of applied working load for F.S= 3, 2.5 and 2 cases, respectively. After excavation, pile shaft shared 55%, 58% and 62% of applied working load for F.S= 3, 2.5 and 2 cases, respectively. It can be noticed that as the working load increases the sharing ratio of pile shaft from the load increases slightly, also the sharing ratio of pile shaft before excavation was less than after excavation.

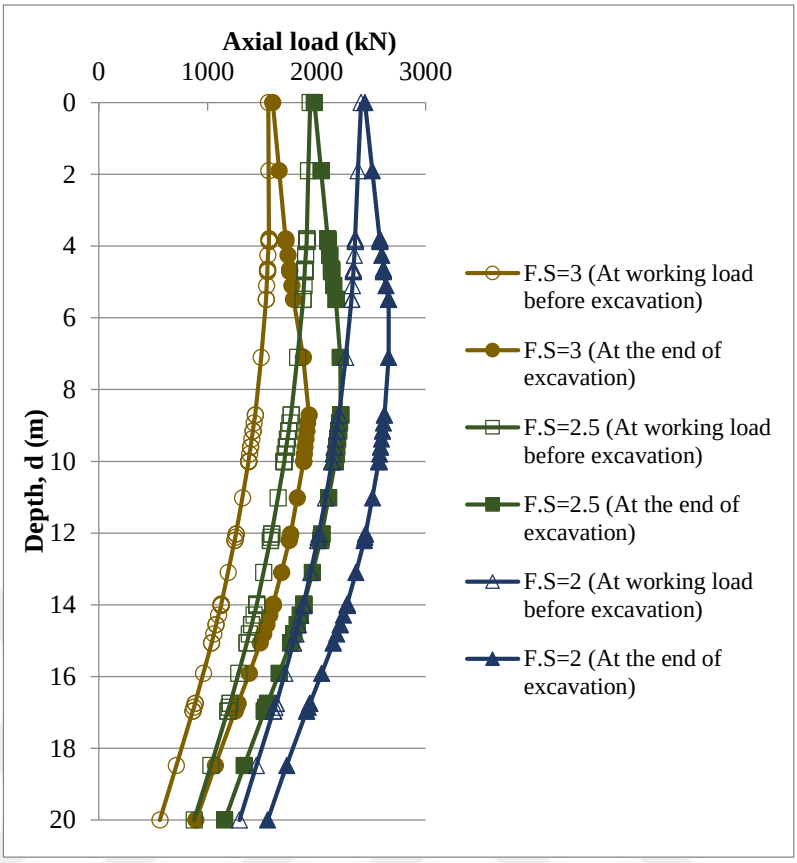

Figure 4.15. Axial load distribution along the pile shaft before and after the excavation at different F.S. in the case of H_e/L_p= 0.5.

From Figure 4.16 it can be noctied that the settlement along the pile increases with the increasing of working load. The settlement increased from 10 mm to 17 mm (1% and 1.7% d_p) with increasing ratio of 70% when the F.S. decreased from 3 to 2. On the other hand, it was noticed that for the increasing applied working load has no effect on the LD and BM of pile as shown in Figure 4.17.a and b.

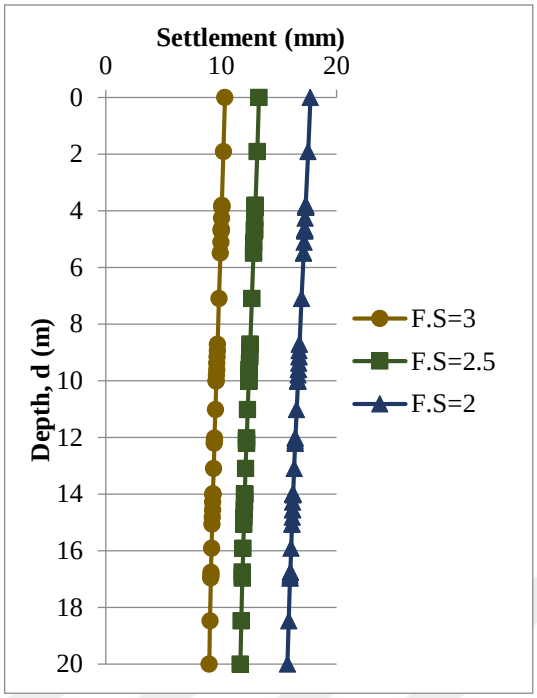

Figure 4.16. The settlement along the pile shaft for different F.S. in case of H_e/L_p= 0.5.

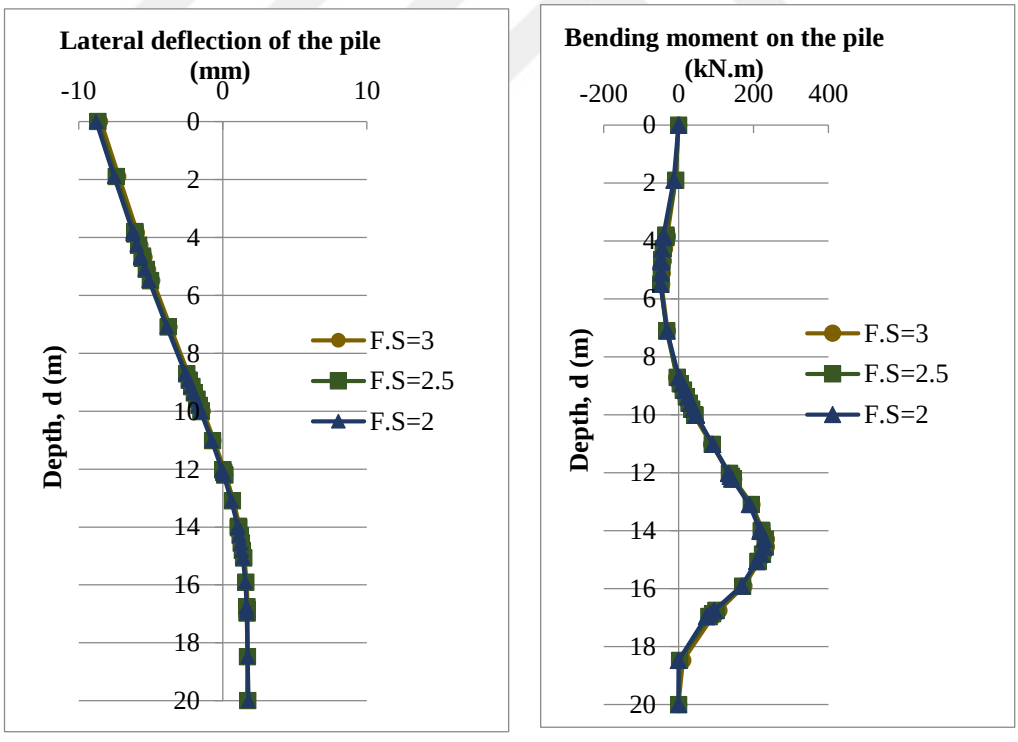

(a) (b)

Figure 4.17. (a) LD of the pile (b) BM on the pile for different F.S. in case of H_e/L_p= 0.5.

4.5. Influence of the pile head type

Figure 4.18.a, b and c illustrates the lateral deflection of pile owing to the excavation in case of free, hinged and rigid pile head for the case of H_e/L_p= 0.5, 1 and 1.5, respectively. The hinged head represents the case of pile group which connected with a beam, while the rigid head represents the case of piles restrained by a rigid raft. It can be observed from the figure that the deflection at the pile head was zero in the case of rigid head for the three cases as expected. This is because of the pile head is restrained from any movement in horizontal and vertical directions. Generally, in the case of hinged and rigid head, the pile deflection is smaller in the upper portion of the pile (about $0.5L_p$) than that of the free head case. Also it can be noticed that the maximum deflection was about at the pile mid-depth in the case of H_e/L_p= 1, while in the case of H_e/L_p= 1.5 the maximum deflection was at the pile toe for all pile head conditions.

Ng. et al. (2017) conducted a centrifuge test (the depth of excavation was 8 m with 2 levels of soft struts and pile length of 20 m) for a rigid head of pile, which is similar to the case of H_e/L_p= 0.5 and the results are shown in Figure 4.19 for comparison. The same figure also shows the centrifuge test results done by Leung et al. (2000) (the excavation depth was 4.5 m with no struts and pile length was 12.5 m). From the figure, it can be noticed that the pile moves totally towards the excavation and the deflection profile is similar for both centrifuge tests. But the lateral deflection in the case of H_e/L_p= 0.5 differs slightly from these centrifuge test results, this is may be attributed to the soft struts and the wall properties that used in the tests.

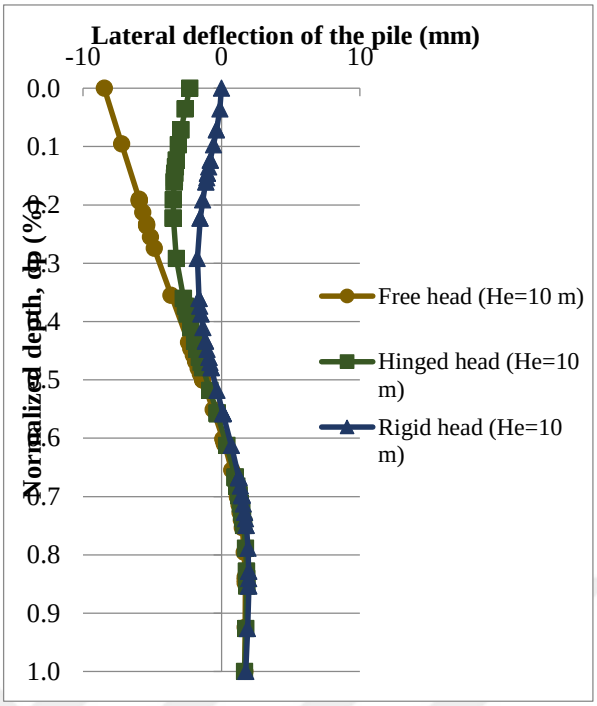

(a)

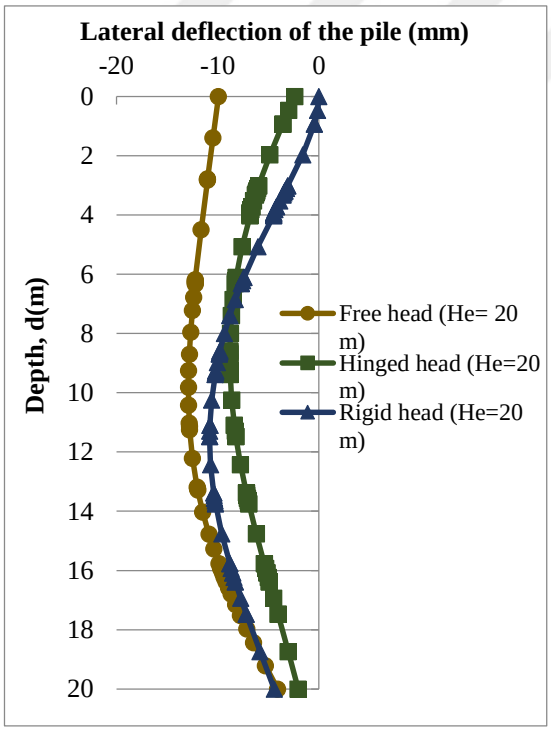

(b)

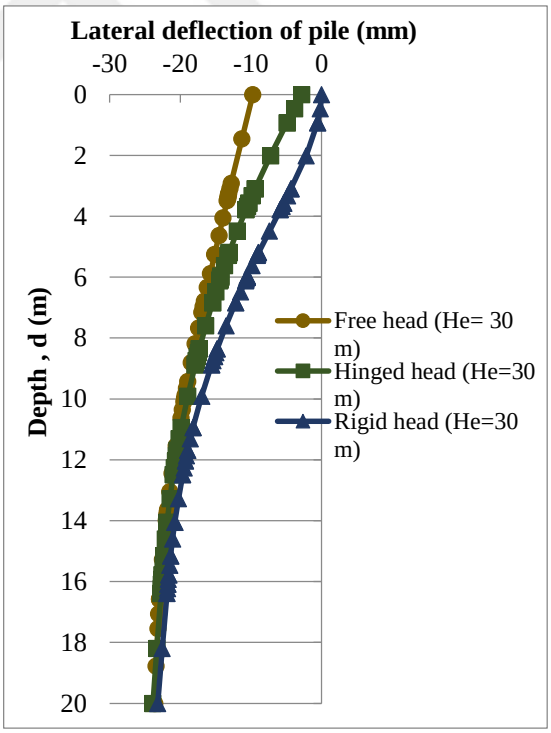

(c)

Figure 4.18. Lateral deflection of the pile in case of free, hinged and rigid pile head for case of (a) H_e/L_p= 0.5 (b) H_e/L_p= 1 (c) H_e/L_p= 1.5.

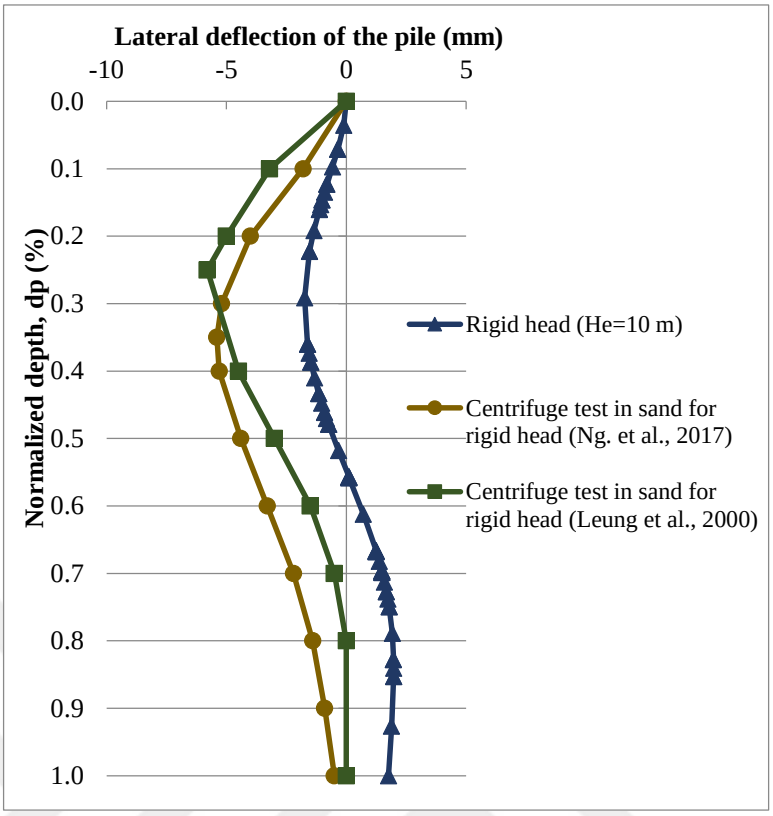

Figure 4.19. Comparison of computed and measured lateral deflection of pile in case of rigid pile head.

Figures 4.20.a, b and c illustrates the generated BM of pile in case of free, hinged and rigid pile head for three cases of H_e/L_p= 0.5, 1 and 1.5, respectively. The negative values mean that the pile is subjected to tensile stress along the pile shaft. A large positive BM was generated at the pile head owing to the restriction of pile head movement in the case of a rigid head. From figures, it was noticed that the generated positive BM at the pile head increases with increasing of H_e. Among the three cases, the positive bending moment was 1927 kN.m (i.e., 154% from pile bending capacity) in the case of H_e/L_p= 1.5 and 1507 kN.m (i.e., 120% from pile bending capacity) in the case of H_e/L_p= 1, respectively, both exceed the pile bending capacity of 1250 kN.m, which is equivalent to 1% steel. (ACI Committee 318, 2005). Hence it can be concluded that the pile head type and excavation depth effects significantly the pile response during the excavation, especially in rigid pile head case where high positive bending moment induces at the pile head, which can exceed the bending capacity of the pile.

For comparison reason, results from two centrifuge tests that mentioned above were included in the Figure 4.21.a. According to the figure it can be obviously noticed that the tests results have the same trend of generated bending moment in case of rigid and hinged head in case of H_e/L_p= 0.5, because the tests were similar to H_e/L_p= 0.5 case expect the used support system stiffness was different. However, the results obtained by Ng. et al. (2017) were higher then the bending moment in case of rigid and hinged head, this can be attributed to support system stiffness that used in the tests.

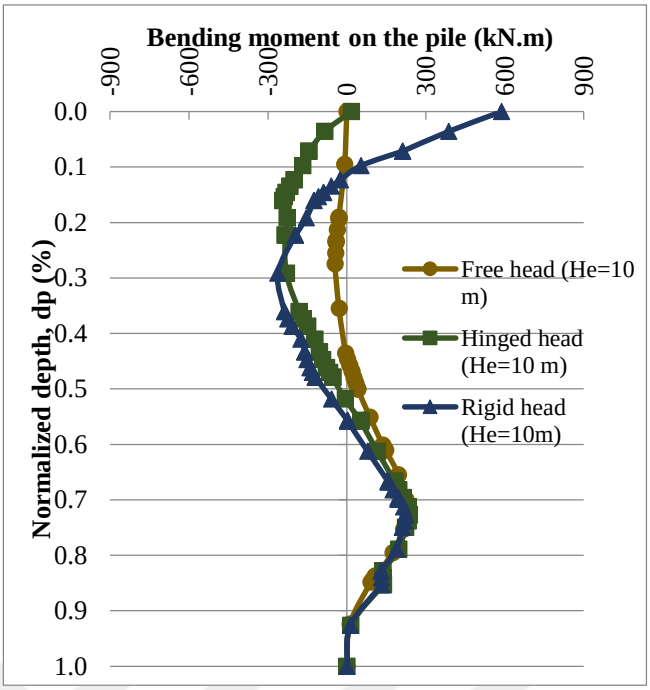

(a)

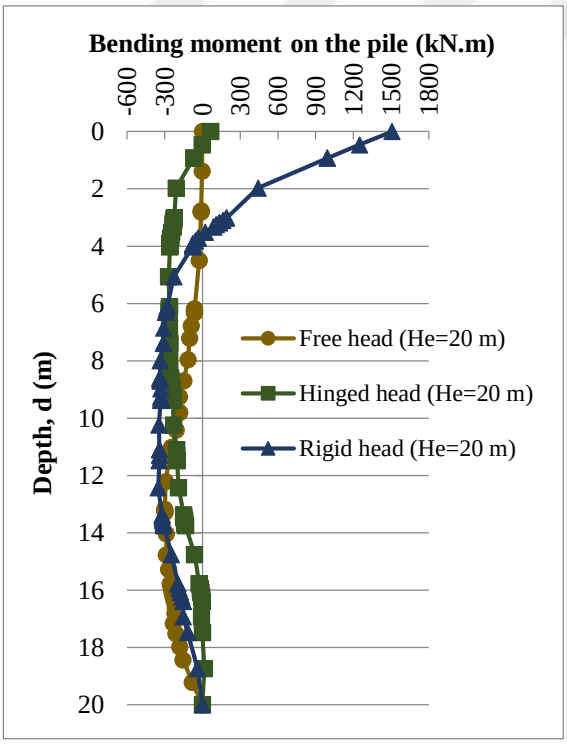

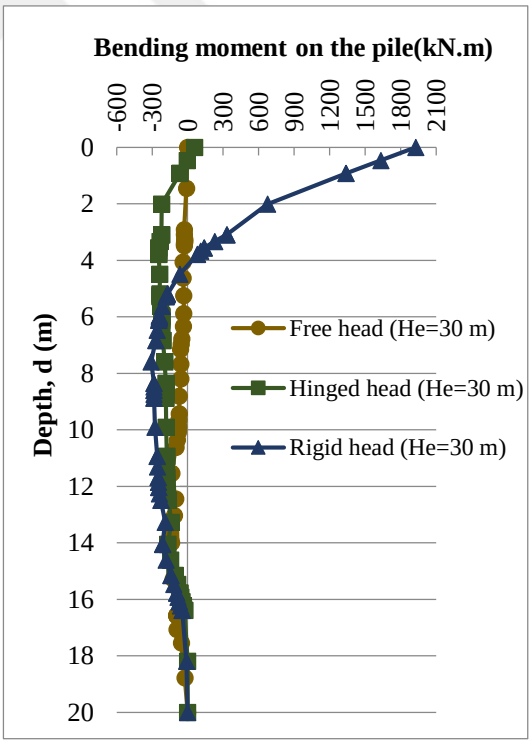

(b) (c)

Figure 4.20. Bending moment on the pile in case of free, hinged and rigid pile head for the case of (a) H_e/L_p= 0.5 (b) H_e/L_p= 1 (c) H_e/L_p= 1.5.

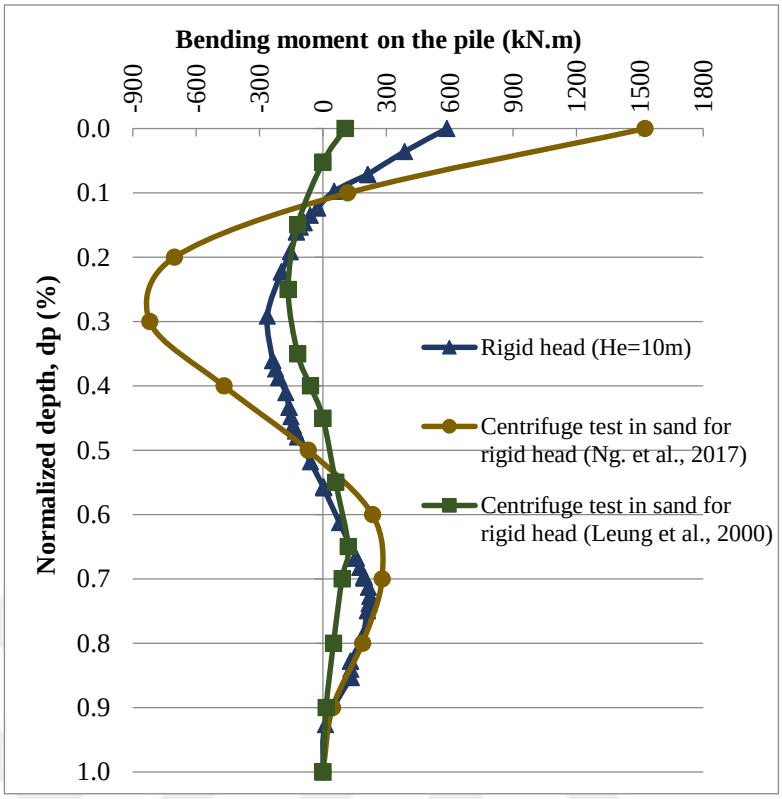

Figure 4.21. Comparison of computed and measured bending moment of pile in case of rigid pile head.

5. CONCLUSIONS

In this study, three dimensional finite element method was performed to evaluate a loaded single pile behaviour in saturated cohesionless soil owing to adjacent deep excavation by using Plaxis 3D software. After verification of finite element model by using centrifuge test results found in literature; a parametric study was conducted to evaluate the influence of some factors on pile behaviour such as excavation depth, distance from pile to the excavation site, pile head type, pile length and working load applied on the pile. Based on finite element analyses results, the following conclusions can be drawn:

- In free-field condition, the ground surface settlement (GSS) behind the wall affected by excavation depth (H_e) significantly and the settlement curve become deeper as H_e increases. Moreover, the ground movement increases significantly as the H_e increases and it decreases when the distance from the wall decreases.

- It is seen that the pile behavior is influenced by the depth of excavation significantly. Among the three cases of H_e/L_p, the case of H_e/L_p= 1 generates the maximum BM in the pile because the pile toe was at the same level with the excavation. While the case of H_e/L_p= 0.5 develops more bending moment with respect to the case of H_e/L_p = 1.5, because H_e/L_p = 0.5 experienced higher restraint from the surrounding soil more than that in case of H_e/L_p= 1.5. On the other hand, the case of H_e/L_p= 1.5 generates the maximum lateral deflection because of the relatively larger H_e/L_p with respect to the other cases.

- As the distance between the pile and the excavation site (X) increases, the lateral deflection of the pile reduces considerably as well as the deflection profile totally changes from curve to a line as the distance increases. On the other hand, after 9 m, the bending moments in the pile are negligible.

- The pile head type has an important effect on the pile behaviour. A significant positive moment was induced at the pile head in case of rigid head pile and it exceeds the bending capacity of the pile (i.e., 154 and 120% from bending capacity of pile) in case of H_e/L_p= 1 and 1.5, respectively. Among the three cases of H_e/L_p; the case of H_e/L_p= 1.5 generates the maximum BM at the pile head for rigid head conditions.

- Increasing the pile length has no influence on the lateral behavior of the pile. The above portion of the pile induced negative bending moment and the below portion of the pile exposed to positive bending moment. Positive bending moment starts approximately after 20 m of pile length, which is the excavation depth and the positive moment increases by the pile length after that point.

- Increasing the amount of applied working load to the pile head has no influence on the lateral behavior of the pile, but has effects on the load distribution. The sharing ratio of pile shaft before excavation is less than after excavation. Moreover, as the working load increases the load sharing ratio of the pile shaft also increases slightly.

Thus it can be said that the depending on the distance and depth of the excavation and also depending on the soil and pile properties, a new excavation site may effect the stability of the existing pile structure severly if the necessary precautions are not taken.

Based on results and conclusions of the this study, it can be recommend that: the geotechnical designer must take into consideration all the factors affecting the safety of the structures which supported on pile foundations that are located next to the deep excavations in sandy soil during the design. It’s worth noting that there are other factors that affect the behavior of piles adjacent to deep excavations that were not studied during this study, such as, the stiffness and type of the support system. It’s suggesting to study these factors in the future studies. Also, it’s suggesting to study the influence of deep excavation on pile group behavior connected by raft foundation.

REFERENCES

ACI Committee 318 (2005). *Buliding code requirements for structural concrete and commentary*.

Akbay Z. (2009). *Yatay yüklü grup kazıkların analizi*. Yüksek Lisans Tezi, YTÜ. Fen Bilimleri Enstitüsü, İnşaat Mühendisliği Anabilim Dalı, İstanbul.

Bowles J.E. (1988). *Foundation analysis and design*, fourth edition. McGraw-Hill Book Company, New York.

Bowles J.E. (1996). *Foundation analysis and design*, fifth edition. McGraw-Hill Book Company, New York.

Broms B. (1964)a. *The lateral resistance of piles in cohesive soils*. J. Soil Mech. Found. Div., ASCE, 90, (SM2): 27-63.

Broms B. (1964)b. *The lateral resistance of piles in cohesionless soils*. J. Soil Mech. Found. Div., ASCE, 90, (SM3): 123-156.

Broms B. (1965). *Design of laterally loaded piles*. ASCE Journal of the Soil Mechanics and Foundations Division, 91, (SM3): 79-99.

Choudhury D., Shen R.F., Leung C.F., Chow Y.K. (2006). *Centrifuge model study on pile responses due to adjacent excavation*. ASCE Gsp 153, 145–151.

Clough G.W., O'Reurke T.D. (1990). *Construction-induced movements of in situ walls*. In Proceedings, Design and Performance of Earth Retaining Structures, ASCE Special Conference, Ithaca, New York, pp. 439-470.

Coduto D.P. (2001). *Foundation design: principles and practices*, second edition. Prentice Hall, Upper Saddle River NJ, 885 pp.

Das B. (2011). *Principles of foundation engineering*, seventh edition.

Davisson M.T. (1970). *Lateral load capacity of piles*. Highway Research Record. Washington, DC: 104-112.

Ding W., Qiao Y. (2014). *Numerical Analysis of Pile Response to Deep Excavation in Soil Overlying Rock.* J. Tunneling and Underground Construction, 700–709.

Finno R.J., Lawrence S.A., Allawh N.F., Harahap I.S. (1991). *Analysis of performance of pile groups adjacent to deep excavation*. J. Geotech. Eng.;117(6):934-55.

Japanese-H-Sections.pdf (fistco.net).

Goh A.T.C., Wong K.S., Teh C.I., Wen D. (2003). *Pile response adjacent to braced excavation*. J. Geotech. Geoenvrion.;129(4):383-6.

Hsiung B.C.B. (2009). *A case study on the behaviour of a deep excavation in sand*. Comput. Geotech. 36 (4), 665-675.

Leung C.F., Chow Y.K., Shen R.F. (2000). *Behavior of pile subject to excavation-induced soil movement*. J. Tunneling and Underground Space Technology, November, 947–954.

Leung C.F., Lim J.K., Shen R.F., Chow Y.K. (2003). *Behaviour of pile Groups subject to excavation-induced soil movement*. J. Geotech. Geoenviron. Eng. 2003(129): 1(58), 58-65.

Li L., Hu X., Dong G., Liu J. (2014). *Three-Dimensional Numerical Analyses of Pile Response due to Braced Excavation-Induced Lateral Soil Movement*. J. Applied Mechanics and Materials.

Liyanapathirana D.S., Nishanthan R. (2016). *Influence of deep excavation induced ground movements on adjacent piles*. J. Tunneling and Underground Space Technology, 52, 168–181.
Ng C.W.W., Yau T.L.Y., Li J.H.M., Tang W.H. (2001). *New failure load criterion for large diameter bored piles in weathered geomaterials*. J. Geotech. Geoenvrion. Eng,., ASCE 127 (6), 488-498.
Ng C.W.W., Poulos H.G. (2017). *Effects of multipropped excavation on an adjacent floating pile*. J. Geotech. Geoenviron. Eng. 143 (7), 04017021.
Nishanthan R., Liyanapathirana D.S., Leo C.J. (2016). *Shielding effect in pile groups adjacent to deep unbraced and braced excavations*. J. Geotech. Eng. 2016:1-13.
Ong D.E., Leung C.F., Chow K.Y. (2006). *Pile behavior due to excavation-induced soil movement in clay. I: Stable Wall*. J. Geotech. Geoenviron. Eng. 2006: 132, (1), 36-44.
Ou C.Y. (2006). *Deep excavation: theory and practice*. Taylor & Francis/Balkema.
Peck R.B. (1969). *Deep excavation and tunneling in soft ground*. In proceedings of the 7th International Conference on Soil Mechanics and Foundation Engineering, State of the Art Volume, Mexico City, pp. 225-290.
PLAXIS Material Models CONNECT Edition V20.
PLAXIS References Manual Edition V20.
Poulos H.G., Davis E.H. (1980). *Pile foundation analysis and design*. Wiley, NewYork, 397 pp.
Poulos H.G., Chen L.T. (1996). *Pile response due to unsupported excavation-induced lateral soil movement*. J. Canada Geotech. 33: 670-677.
Poulos H.G., Chen L.T. (1997). *Pile response due to excavation-induced lateral soil movement*. J. Geotech. Geoenviron. Eng. 1997; 123:382-8.
Shakeel M., Ng C.W.W. (2017). *Settlement and load transfer mechanism of pile group adjacent to a deep excavation in soft clay*. Comput. Geotech. 96, 55-72.
Soomro M.A., Mangnejo D.A., Bhanbhro R., Memom N.A. (2019). *3D finite element analysis of pile responses to adjacent excavation in soft clay: Effects of different excavation depths systems relative to a floating pile*. J. Tunnelling and Underground Space Technology.
Teh K.L., Leung C.F., Chow Y.K. (2005). *Spudcan penetration in sand overlying clay*. ISFOG 2005, Perth, Australia, pp. 529-534.
Tomlinson M., Woodward J. (2008). *Pile design and construction practice*, fifth edition.
Ünsever Y.S. (2015). *An experimental study on static and dynamic behaviour of model pile foundations*. PhD thesis, ODTÜ Fen Bilimleri Enstitüsü, İnşaat Mühendisliği Anabilim Dalı, Ankara.
Venkatramaiah C. (2006). *Geotechnical engineering*, third edition.
Zeevaert L. (1957). *Compensated friction-pile foundation to reduce the settlement of buildings on highly compressible volcanic clay of Mexico City*. Proc. 4 ICSMFE, London.
Zhang R., Zhang W., Goh A. (2018). *Numerical investigation of pile responses caused by adjacent braced excavation in soft clays*. J. Geotech. Engineering.